Marine Chemistry
July 2022, Volume 244 Pages 104139 (13p.)
https://doi.org/10.1016/j.marchem.2022.104139
https://archimer.ifremer.fr/doc/00776/88754/

Rapid and simple determination of iron-porphyrin-like complexes (Fe-Py) in estuarine and marine waters

Laës-Huon Agathe [1, *], Davy Romain [1], Thomas Léna [1], Devesa Jeremy [2], Hemery Alexandre [1], Waeles Mathieu [2], El Rakwe Maria [1], Riso Ricardo [2], Dulaquais Gabriel [2]

[1] Unité recherches et développements technologiques Ifremer, RDT, F-29280 Plouzané, France
[2] Laboratoire des sciences de l'environnement marin, Univ Brest, Ifremer, CNRS, IRD, LEMAR, F-29280 Plouzané, France

* Corresponding author : Agathe Laës-Huon, email address : agathe.laes@ifremer.fr

Abstract :

This work presents a new method for determining iron-porphyrin-like complexes (Fe-Py) based on Continuous Flow Analysis (CFA) with chemiluminescence detection and its application to natural waters in an estuarine environment. The involved reaction is founded on luminol oxidation by hydrogen peroxide in the presence of Fe-Py complexes at pH 13. The detection limit is 7.2 pM hemin equivalent, the linear range extends to 150 nM and precision of the method is 6.4% at 0.25 nM (n = 8). This new method's detection limit is 15 times lower than the previous analytical procedure of Vong et al. (2007), based on Flow Injection Analysis (FIA) and using different chemical conditions. Moreover, the presented method is fast (90s/analysis), involves a low consumption of reagents, a small sample volume, and simplified sample handling. The method was applied to natural samples collected along the temperate macrotidal Aulne estuary (Bay of Brest, France). Here, we report for the first time on the spatial distribution of the Fe-Py complex concentration (dissolved, reactive particulate) over the entire salinity gradient of a macrotidal temperate estuary. The Fe-Py concentrations in the riverine and marine end-members were 0.873 ± 0.007 nM (S = 0.92) and 0.010 ± 0.004 nM (S = 34.86), respectively. Between these two salinities, non-conservative behaviour was observed, with an increase in Fe-Py concentrations to 1.142 ± 0.031 nM at S = 5.2 corresponding to the Maximum Turbidity Zone (MTZ), followed by a strong removal of Fe-Py in the salinity range 5–20. Then, the Fe-Py concentrations decreased linearly during mixing processes, reaching picomolar levels towards the coastal waters. The estimated entering flux from the river equaled 240 ± 2 g.d−1 whereas the net flux to coastal sea waters was 95 ± 10 g.d−1 leading to a loss of ~60%. The estuarine system globally acts as a sink for Fe-Py complexes, probably due to the aggregation of Fe-Py complexes on particles, to flocculation and/or sedimentation

Highlights

► Rapid and simple detection of Fe-Py complexes was developed for marine waters. ► Fe-Py complexes distribution was reported for the first time in a salinity gradient. ► Aulne estuary acts as a sink for Fe-Py, decreasing their input to the Atlantic Ocean.

Keywords : Iron, Heme, Porphyrin, Estuary, Continuous flow analysis

1- Introduction

The importance of iron (Fe) in the oceanic carbon cycle has been clearly established through biogeochemical processes (Anderson, 2005). Iron is unquestionably one of the factors limiting primary production in more than 40% of the world ocean (de Baar et al., 2005; Geider and La Roche, 1994; Moore et al., 2013). Despite advances in Fe biogeochemical involvement, there is an acute lack of data on its physico-chemical speciation in natural waters.

Its stabilisation in the water column, transport, transfer to the sedimentary compartment and capacity to be assimilated by marine microorganisms differ (Tagliabue et al., 2017) according to its form (free, inorganically or organically complexed). Iron is found in particulate, (PFe, >0.45 µm), dissolved (dFe, < 0.45µm), soluble (sFe, < 0.02µm) and colloidal (cFe, between 0.45 and 0.02µm) forms, operationally defined by the pore size of the filtration membrane (Worsfold et al., 2014). Dissolved iron is itself divided into two categories: free iron and complexed iron (Turner and Hunter, 2001). The scientific community currently supports that dissolved iron is more than 99% complexed with organic ligands in oxygenated seawater (Gledhill and van den Berg, 1994; Witter et al., 2000) and estuarine waters (Batchelli et al., 2010; Muller, 2018; Rijkenberg et al., 2006). The organic pool is considered a key feature of iron biogeochemical processes (Völker and Tagliabue, 2015) as it increases the overall iron solubility (Johnson et al., 1997; Liu and Millero, 2002). However, characterisation of iron ligands, organic and inorganic in natural waters, is a major challenge. These ligands can be very different (Gledhill and Buck, 2012), with high concentrations in estuaries (e.g. humic substances, hundreds of $\mu g.l^{-1}$ to $mg.l^{-1}$, Abualhaija et al., 2015; Laglera and Van Den Berg, 2009; Riso et al., 2021) and extremely low concentrations in open ocean waters (e.g. siderophores, nM to pM ,Boiteau et al., 2016; Bundy et al., 2014; Mawji et al., 2008). The ligands have varied sources such as terrestrial breakdown of plant materials: these can be produced *in situ* or degraded by different microorganisms. Natural waters can therefore contain a mixture of ligands such as siderophores (Bundy et al., 2018; Mawji et al., 2011; Vraspir and Butler, 2009), inorganic nanoparticles (Lough et al., 2019; Yücel et al., 2011), humic substances (Abualhaija et al., 2015; Dulaquais et al., 2018; Whitby et al., 2020) and/or porphyrins (Louropoulou et al., 2020, 2019; Vong

et al., 2007). According to their intrinsic nature, they can form strong and weak complexes with iron, such a qualification being operationally defined by competitive equilibrium voltammetric experiments (Gledhill and van den Berg, 1994; Witter et al., 2000). Witter et al., (2000) suggest that most unknown ligands in seawater could originate from porphyrin and siderophore-like compounds. Porphyrins, which include chlorophylls, chlorophyll breakdown products like phaeophytin, hemes, and vitamin B12, are produced by almost all living organisms (Gledhill and Buck, 2012). Hemes participate as enzymatic cofactors in processes like photosynthesis (cytochromes, globin), electron transfer (catalases, cytochromes P450, peroxidases), respiration, and nitrate assimilation (nitrate reductase, Hogle et al., 2014). Iron-porphyrin-like complexes such as heme b (Fe protoporphyrin IX) in seawater probably result from cell lysis, either through grazing or viral attack. (Witter et al., 2000) used tetrapyrrole molecules (phaeophytin, protoporphyrin IX and protoporphyrin IX dimethylester) to represent Fe-binding organic complexing ligands released into seawater from bacteria and phytoplankton degradation as part of their model. (Laglera et al., 2020) also suggest that the recycled iron ligands observed in their study were probably released during grazing and copepod fecal pellet cycling. They indicate that intracellular ligands such as hemes (pigments containing the iron binding moiety porphyrin) could be the cause of this class of ligands but without being able to characterise the true nature of these organic molecules. The different type of ligands could be released into the medium via cell lysis during sloppy grazing and recycling of fecal pellets (packed with phytoplanktonic cells). Despite their ubiquity in natural waters, Fe-Py compounds have been less studied than siderophores in the ocean. They are considered weaker binding ligands (Hassler et al., 2017; Schlosser and Croot, 2008; Völker and Tagliabue, 2015) with very low solubility in seawater at pH 8 (Gledhill, 2007; Gledhill and Buck, 2012). However, several studies (Bellworthy et al., 2017; Isaji et al., 2020) have shown that heme and hemoproteins are relevant complexes in iron biogeochemical cycling as they persist in seawater and on marine particles. Recently, Hogle et al., (2014) and Louropoulou et al., (2020, 2019) highlighted the importance of such ligands in the iron biogeochemical cycle presenting an extensive dataset of particulate heme b abundance in the Atlantic Ocean. The authors suggest that heme b could account for between 0.17–9.1% of biogenic iron, a significant portion of the total biogenic iron pool in the Atlantic Ocean. The quantification of particulate heme b can be attained through High-Performance Liquid Chromatography (HPLC) – Diode Array Detection (DAD) or Electrospray Ionisation (ESI) - Mass spectrometry (MS) after solvent extraction (Gledhill, 2014, 2007; Gledhill et al., 2013; Louropoulou et al., 2020, 2019). These techniques present undeniable advantages in terms of sensitivity, reaching low detection limits ranging from 9 pM (Bellworthy et al., 2017) to 0.01-0.02 pM (Louropoulou et al., 2020) enabling the analysis of most seawater conditions. However, the overall heme b determination involves several steps of extraction and analysis. In 2007, Vong and co-authors published a method for determining

iron-porphyrin complexes based on flow injection analysis (FIA) and chemiluminescence detection using hemin (Chloroprotoporphyrin IX iron (III)). These authors were able to detect heme-like compounds, called iron-porphyrin-like (Fe-Py) complexes in the Rhone river and the Berre pond. However, their detection limit (0.11 nM) did not allow the detection of Fe-Py complexes in the surface waters of the Southern Ocean.

In this study, we have optimised the method developed by Vong et al., (2007), moving from the flow injection technique to continuous flow analysis (CFA) with the addition of hydrogen peroxide as the reaction oxidant. Various interferences (organic and metallic compounds, pH, and salinity) were tested and figures of merits determined according to method modifications. This rapid method (90s/analysis) was applied to natural unfiltered samples collected along the land-sea continuum of a temperate macrotidal estuary (Aulne estuary, Bay of Brest, France), reporting for the first time Fe-Py (dissolved + reactive particulate) distribution throughout an entire estuarine system.

2- Experiment

The method used to analyse iron-porphyrin-like complexes (Fe-Py) is based on chemiluminescent detection and is derived from the work of Vong et al. (2007). The reaction relies on luminol oxidation in the presence of Fe–Py complexes at pH 13. The new reagent and apparatus conditions are described in the following paragraphs.

The concentrations of dissolved (DFe) and soluble iron (SFe) were obtained using a FIA technique based on colorimetric detection. This method is described in previous papers (Laës et al., 2005; Measures et al., 1995). Briefly, iron contained in an on-line buffer sample, is previously concentrated on a column, then eluted using hydrochloric acid (30% Sigma Aldrich suprapur ®) diluted at a concentration of 0.11M in artificial seawater. The flow then passes through the manifold and the iron present in the carrier acts catalytically on the oxidation reaction of the amine (N,N-dimethyl-p-phenylenediamine (4-amino-N,N-dimethylaniline)dihydrochloride, Sigma Aldrich) at a specific pH of 9 in presence of hydrogen peroxide (H_2O_2, 30% Suprapur, Merck) at a concentration of 1.6M. The detection limit for dissolved and soluble Fe detection by FIA was estimated to be 20.11 nM for direct sample determination and 0.13 nM when preconcentration step was used.

The Particulate Organic Carbon (POC) analysis was performed using a Thermo Flash 2000 elemental analyser (combustion of the sample packed in a tin combustion boat at 950°C, separation of the combustion gases via a gas chromatography column, then detection via a catharometer (Thermal Conductivity Detector, TCD)). The apparatus was calibrated according to several acetanilide

standards. For chlorophyll and pheophytin analysis, we followed the protocol developed by (Yentsch and Menzel, 1963). The sample filter was extracted in 90/10 acetone, and then stored in a cool and dark place for 12 hours. The fluorescence of the extract was than measured before and after acidification with HCl 0.1 M using a Turner Designs (10-AU) system with excitation and emission wavelengths of 450nm and 670nm, respectively.

2.1- Chemicals and reagents

2.1.1- Fe-Py determination

Aqueous solutions were prepared with ultrapure water (resistivity > 18.2 MΩ, Milli-Q 93 Element System, Millipore®, called UP-water hereafter). The method for determination of Fe -Py compounds is not as prone to contamination as iron analysis (Hogle et al., 2014). However, because metallic interference was studied and in pursuance of Fe-Py measurement quality, every plastic container was previously cleaned with hydrochloric acid 30% (Sigma Aldrich suprapur ®, pH 2), and rinsed three times using UP-water before being used for reagent preparation and sample collection. The same procedure was also applied to iron determination.

The alkaline luminol solution ($1.5.10^{-3}$ M) was prepared by dissolving 10 g of sodium hydroxide (Sigma-Aldrich®) in 300 ml of UP-water, then 88.6 mg of 5-amino-2,3-dihydro-1,4-phthalazinedione (Aldrich®) and 900 µL of linoleic acid (Fluka®) were added. The final solution was stirred until total dissolution before being completed to 500 ml. It was prepared the previous day and stored in the dark. The EDTA solution (0.25 M) was prepared in 1 l of UP-water to which were added 89.52 g of Ethylenediaminetetraacetic acid, trisodium salt hydrate (Across Organics®). The hydrogen peroxide solution (0.7 M) was obtained by diluting 35.75 ml of H_2O_2 (for trace analysis Fluka®) in 500 ml of UP-water.

The Fe-Py standards were prepared by diluting a stock solution of $1.5.10^{-3}$ M hemin (Chloroprotoporphyrin IX iron(III)). As described in Vong et al. (2007), the concentrations of Fe-Py complexes were determined by standard additions of hemin in artificial seawater. Consequently, concentrations of Fe-Py complexes are expressed in nanomolar of hemin equivalent. The stock solution was prepared by dissolving 0.0978 g of hemin (Sigma-Aldrich) in 100 ml of an alkaline solution of 0.1 M of sodium hydroxide. It was prepared daily, kept in the dark and at a low temperature. Tests were performed on the hemin response from a stock solution of hemin immediately, three hours and six hours after its preparation. No statistical differences were observed between the different tests. A daughter solution of hemin (2.4 µM) was prepared by diluting 80 µl of the stock solution in 0.1 M of sodium hydroxide. This solution was prepared daily and stored in the

dark. Artificial seawater (1l) was prepared from ten salts (NaCl © Suprapur: 23.9g, $MgCl_2$ $6H_2O$ © Normapur Analar: 10.8g, Na_2SO_4 © Normapur Analar: 4g, $CaCl_2$ $2H_2O$ © Emsure ACS : 3.08g, KCl ACS reagent: 0.7g, $NaHCO_3$ © Normapur Analar: 0.2g, $SrCl_2$ $6H_2O$ © Normapur Analar: 0.025g, KBr © Emsure ACS: 0.1g, H_3BO_3 © Rectapur: 0.03g, NaF © Normapur Analar: 0.003g) dissolved in UP-water as indicated in Aminot and Kerouel (2007). Simplified artificial seawater (1 l) was composed of three salts (NaCl © Suprapur: 24.53 g, $MgCl_2$ 6 H_2O © Normapur Analar: 11.1 g, Na_2SO_4 © Normapur Analar: 9.4 g, $CaCl_2$ 2 H_2O © Emsure ACS: 1.54 g) dissolved in UP-water. Before analysis, standards and samples were buffered using a mixture of NH_3/NH_4 pH 9.5, prepared with 75 ml of suprapure® ammonia solution 25% (Merck) and 53 ml of suprapure® hydrochloric acid 30% (Merck).
Nanomolar hemin standards were prepared by diluting the daughter solution in 10 ml of artificial seawater. A sample buffer of 750 µl was added to the standard solution before being pumped by the CFA apparatus. The same procedure was applied to the river, estuarine and seawater samples.

As the analytical method had been modified, the selectivity of this new procedure needed to be checked accordingly. A stock solution of bovine liver catalase (Sigma-Aldrich, 30 µM) was prepared in UP water and a stock solution of horseradish peroxidase (Apollo Scientific, 9 µM) was prepared in a Tris (hydroxymethyl) aminomethane buffer 0.25 M. As for hemin standards, nanomolar concentrations of the proteins were prepared by dilution in 10 ml of artificial water, following the procedure described above.

2.2 Interferences

Interfering metal solutions (100 mM, 25 ml of acidified UP-water pH 2) were prepared from 0.3407 g of zinc chloride ($ZnCl_2$, Sigma-Aldrich), 0.9804 g of ammonium iron (II) sulfate hexahydrate ($Fe(NH_4)_2(SO_4)_2$, 6 H_2O Sigma-Aldrich), 1.2055 g of ammonium iron (III) sulfate dodecahydrate ($FeNH_4(SO_4)_2$, 12 H_2O Sigma-Aldrich), 0.6242g of copper sulfate ($CuSO_4$, $5H_2O$, Sigma-Aldrich) and 0.4948 g of manganese chloride ($MnCl_2$, $4H_2O$, Sigma-Aldrich). Intermediate solutions were prepared to complete the interference tests at different levels, i.e. 0, 350, 700 nM for Fe^{3+}, $Zn^{2+}$and Mn^{2+} ; 0, 50, 100 nM for $Cu^{2+}$and 0, 25, 50 nM for Fe^{2+}.

Two humic substances, three porphyrins (different from hemin), and three siderophores were tested as interfering organics. Humic substances were Elliot Soil Fulvic Acid (ESFA) and Suwannee River Fulvic Acid (SRFA, 4500 µgC/l, IHSS). Humic solutions were prepared by diluting a 256.12 $mg.l^{-1}$ stock solution (prepared by dissolving a dried mass of SRFA and ESFA in milliQ solution). Siderophore solutions were composed of ferrioxamine E (*Streptomyces antibioticus,* Sigma-Aldrich), deferoxamine for peak identifications CRS 1 (Sigma-Aldrich, metal uncomplexed), and a mixture of pyoverdine

(Sigma Aldrich P8124) mainly composed of succinic acid and succinimide. Siderophore solutions were prepared by dissolving respectively 1 mg of each compound in 100 ml of UP water. Daughter solutions of 6.67 nM were prepared to spike 10 ml of artificial seawater to reach 10 and 20 pM final concentrations for the interference tests. The three other porphyrin-like molecules tested were: (1) a magnesium complexed molecule: chlorophyll *a* (from spinach, Sigma Aldrich), (2) protoporphyrin IX (3,7,12,17-Tetramethyl-8,13-divinyl-2,18-porphinedipropionic acid, Sigma Aldrich), and (3) a manganese complexed porphyrin: 5,10,15,20-Tetraphenyl-21*H*,23*H*-porphine manganese (III) chloride (Sigma Aldrich). The Fe-Py solutions were prepared as for the stock solution of hemin using 0.1 M sodium hydroxide. The masses were 0.0844 g for protoporphyrin IX and 0.1054 g for manganese complexed porphyrin. Finally, a chlorophyll-*a* solution (1 mg bulb Sigma Aldrich) was diluted in 100 mL 90% acetone. The final concentrations tested were supposed to be similar to those expected in an estuary media. Siderophores were tested at a final concentration of 0, 10 and 20 pM, porphyrins 0, 1 and 2 nM, Chlorophyll-*a* 0, 25 and 50 $\mu g.l^{-1}$, and humic substances 0, 2250, and 4500 $\mu g.l^{-1}$ for the Elliott Soil Fulvic Acid and 0, 1125 and 2250 $\mu g.l^{-1}$ for the Suwannee River Fulvic Acid.

An interference test with Fe particles was performed with two solutions containing Fe_2O_3 at concentrations of 3.25 and 6.5 µM in artificial seawater, these solutions being prepared by diluting a stock solution made with 0.215g ferric oxide (Fe_2O_3, Sigma Aldrich powder < 5µm > 96%) in 100 ml UP water. The interference test with Fe colloids was performed with two solutions containing 0.35 and 0.7 µM of $FeCl_3$ in artificial seawater; these solutions being prepared after two consecutive dilutions of a stock solution made with 0.219g of $FeCl_3$ in 100ml of artificial seawater. The different stock solutions used here were maintained unstirred for 24 hours to enable the apparition of colloidal iron. The various interferences tests with Fe particles and Fe colloids were conducted at three different hemin concentrations: 0, 1 and 2 nM.

To complete the interference tests, a certified material for metal concentrations consisting of a powder of freeze-dried plankton from a freshwater pond (IRMM, BCR®-414) was tested. The tested concentrations of the BCR sample were 225 and 450 $\mu g.l^{-1}$. These levels were determined by (1) considering a chl-*a* concentration of 5 µg/l, which is a typical high value for the Bay of Brest system(Le pape et al., 1996) and (2) that purely algal organic matter has a C/Chl-*a* ratio of 40 (Abril et al., 2000). Two types of phytoplankton cells belonging to the common microalgae population in the Bay of Brest were also tested for Fe-Py analysis. Dinoflagellate (*Scrippsiella*) and diatoms (*pseudo nitzschia*) were grown in the Ifremer laboratory. The average abundance for an usual winter period (October) was estimated between $4 * 10^4$ $cells.l^{-1}$ (Queguiner and Tréguer, 1984) and $2.4 * 10^5$ $cells.L^{-1}$ (Beucher et al., 2004). The tested concentrations were thus 1.24 and $2.48*10^5$ $cells.\ l^{-1}$ for the

dinoflagellates and 0.7 and 1.4 * 10^5 cells. l^{-1} for the diatoms. Volumes of fresh cultures were added to the artificial seawater and then treated like other samples.

2.3- Study area and sample collection

2.3.1- Study area

The Bay of Brest and the Aulne river (Brittany, France, Fig.1) have been described in numerous studies (Marie et al., 2017; Raimonet et al., 2013; Riso et al., 2021, 2007; Waeles et al., 2013). Briefly, the Bay of Brest (48°200N; 04°200W, Brittany, France) is a 130-km-long semi-enclosed system connected to the coastal waters of the Iroise Sea by a narrow and deep strait. Its drainage basin covers 1850 km^2 mainly influenced by agricultural activities. The Aulne estuary, the main river discharging into the Bay of Brest, is 35 km long. It is meandering and protected from the coastal influence by the Crozon peninsula. The water flux is primarily controlled by the river flow, 60% of the annual flow generally occurring in the December-March period. It is also dependent on the tidal range (1.2-7.3m) of the Bay of Brest resulting in intense variations in water depth and sediment deposition and erosion in the Aulne estuary (Marie et al., 2017).

2.3.2- Sample collection

Sample collection was operated during the FeLINE cruise (Fer LIgands in AulNe Estuary) on 22 October 2018 onboard the RV *Hésione* (INSU-CNRS-UBO). Twenty sub-surface (0.5 m depth) sampling points were dispatched along the Aulne river (S=0.92) estuary, Bay of Brest, and Iroise Sea (S=34.86) covering the entire land-sea continuum (North Brittany, Atlantic Ocean, France, Fig. 1). The flow rate was minimal for this period with a value of 4.85 $m^3.s^{-1}$, compared to the average October flow rate of 9.71 $m^3.s^{-1}$ (Banque HYDRO, http://www.hydro.eaufrance.fr). The tidal coefficient was also low (39).

The sampling locations were selected with the aim of mapping the entire freshwater—seawater mixing zone. Twelve parameters were studied including Fe-Py complexes which will be discussed here. Conventional physicochemical parameters (T°, S, pH, O_2) were measured in situ using an AQUAread AP-2000 probe calibrated on the day of sampling. The accuracy of the measurements is ± 0.1g kg^{-1} and ± 0.05 pH units for salinity and pH. A Maximum Turbidity Zone (MTZ) characterised by muddy waters was visible to the naked eye for salinities around five. The pH variation was confirmed. Sampling flasks for Fe-Py complexes (nalgene, HDPE, 30ml) were previously cleaned with hydrochloric acid (30%, suprapur®, Sigma Aldrich, pH=2) and rinsed three times with UP water. They

were also rinsed three times with natural water before final collection. Fe-Py unfiltered samples were preserved by the addition of sodium azide (3µl NaN_3, 0.01 M for 30 ml) and stored frozen before analysis. They were analysed in triplicates later in the laboratory using the method described hereafter. The fraction of Fe-Py complexes analysed in the paper will be considered as the dissolved plus the reactive particulate fraction and will be displayed in nM hemin equivalent.

Dissolved iron (DFe) samples were recovered after filtration with 0.45-µm-mixed-celullose ester membranes (HATF, Millipore). Soluble iron (SFe) samples were obtained after filtration of a dissolved aliquot through an Anotop syringe filter (0.02 µm). Both dissolved and soluble fractions were acidified with HCl (30%, suprapur®, Sigma Aldrich, pH=2) and stored in double plastic bags in the dark. The 0.45 µm HATF filters were processed to determine the fraction of particulate iron (PFe) as well as for chlorophyll and pheophytin determination. Dissolved and soluble iron were determined using the flow injection analysis method with colorimetric detection as described in (Measures et al., 1995). The lowest concentrations were detected using a preconcentration column composed of Toyopearl 650M.

2.4- Apparatus

The apparatus used here is derived from the deep-sea chemical analyser CHEMINI (CHEmical MINIaturized analyser), previously described by Vuillemin et al., (2009). This laboratory version is based on Continuous Flow Analysis (CFA) with chemiluminescence detection.

Standards or samples, previously buffered at pH 9, were introduced to the manifold using a peristaltic pump (PA, pump A Fig. 2). They were then mixed with the EDTA (PB, pump B) in the first mixing coil (MC1). EDTA avoided precipitation of the major seawater ions as they met the reagents stream (H_2O_2, luminol, pH 12.6, RC, reaction coil, L=122 mm) pushed by PC (pump C). The mixture passed through the reaction coil before reaching the photomultiplier (PMT H5783-10, Hamamatsu Photonics). Finally, the light emitted from the oxidation of luminol in the presence of Fe-Py complexes was transformed into an electronic signal read on the data manager (Memograph M RSG45, Endress + Hauser). A standard analysis lasted 90 seconds and the voltage signal delivered by the datalogger was averaged over 50 values. The limit of detection was calculated as three times the standard deviation for the analysis of ten replicates of the blank (artificial seawater with buffer addition).

3- Results

3.1- Impact of interferences

3.1.1-Salinity and pH effect

The salinity effect was studied for two standards of hemin (1 and 5 nM) that were prepared in solutions with salinities varying from 2 to 35. The salinities were obtained by mixing artificial seawater with UP water. No statistical difference between the five salinities tested (S2, S5, S20, S25, S35, ANOVA one factor) was noticed, indicating that the analysis of the collected samples will not require any specific precaution regarding salinity.

pH variation along the Aulne transect was estimated between 8.2 and 7.3. The stability of the pH sample once buffered (pH 9.5 once added) was checked at the two pH values without any change in the signal response.

3.1.2- Metallic interferences

The luminol oxidation reaction with hydrogen peroxide under acidic conditions is a well-known detection method for iron in seawater (Laës et al., 2007; Obata et al., 1993; Ussher et al., 2007). The method used here relies on the same process but uses a much higher pH of 13. The addition of EDTA inhibits the precipitation of the major ions of seawater thus permitting analysis of the Fe-Py complexes. It was however necessary to check if the initial metallic ion concentrations in the natural samples were not interfering with the analytical process. Therefore, a central composite design (CCD), using JMP software was conducted to rapidly test the influence of iron (Fe), manganese (Mn), zinc (Zn), and copper (Cu) at concentration levels commonly encountered in estuaries. For Fe^{3+}, $Zn^{2+}$and Mn^{2+}, concentrations of 0, 350 and 700 nM were tested (Ouddane et al., 1999; Rijkenberg et al., 2006; van den Berg et al., 1987). Fe^{2+} and Cu^{2+} concentrations were respectively 0, 25 and 50 and 0, 50 and 100 nM (Bordin, 1991; Rijkenberg et al., 2005). The maximum iron concentrations tested as a potential interferent have been determined according to the results obtained in this study. This test was conducted with three different hemin concentrations: 0, 1 and 2 nM. The final solutions were prepared in artificial seawater. Our results indicated that most of the metallic concentrations tested did not interfere with the analytical signal with and without the presence of hemin (p value < 0.001). Fe^{3+} was the only exception, alone in the solution and coupled with hemin. Further extensive testing was performed using various Fe^{3+} concentrations: 0, 87.5, 175, 350, and 700 nM in the absence or presence of hemin (2 nM). To ensure that the variation in the signal response was only due to Fe^{3+} in

the solution, and not to a hysteresis nor a memory effect, a blank was analysed between each addition of iron. Moreover, the different iron concentrations tested were used randomly. The same procedure was achieved for the analysis of 2 nM + Fe^{3+} solutions. In the presence of 2 nM hemin, none of the Fe^{3+} concentrations impacted the hemin detection. The obtained signals were in accordance with the 2 nM signal detected before and after the analysis of iron (according to method uncertainties). However, in the absence of hemin, Fe^{3+} gave a signal slightly above the blank value for a concentration of 700 nM. The difference in hemin concentration between the sample spiked with 700nM Fe^{3+} and the blank was estimated to be 5 pM hemin equivalent, which is lower than the detection limit. Therefore, it can be considered that Fe^{3+} and the other ambient metallic ions should not impact Fe-Py determination in estuarine or marine waters. As already considered in Vong et al. (2007), the absence of interference by Fe^{2+}, Mn^{2+}, Cu^{2+} and Zn^{2+} on the Fe-Py signal likely results from non-optimum pH conditions.

3.1.3- Organic interference

There are hundreds and even thousands of discrete organic ligand types in seawater but we focused here on the main iron organic ligands already observed in estuarine and coastal waters. These ligands can potentially compete with Fe-Py compounds for the complexation of iron and can also directly affect the analytical response. Three different types of organic ligands were tested: humic substances, siderophores, and porphyrins. Muller, (2018) defines humic substances as complex, acidic organic molecules formed by biotic and abiotic processes following the decomposition of plant and microbial material. They form in soils and the water columns of lakes and oceans and have the potential to complex iron. In the estuarine and the marine environment, their composition and molecular structure can change in space and time making it complex to define a global intrinsic humic structure (Dulaquais et al., 2018; Riso et al., 2021). As they are considered an important component of the ligand pool in estuarine systems (Laglera and Van Den Berg, 2009), two models of humic substances were tested as potential interfering compounds: Elliott Soil fulvic acids (ESFA) and Suwannee River fulvic acids (SRFA). Gledhill & Buck, (2012) described two other biologically produced types of organics as major iron-binding ligands: siderophores and porphyrins. Siderophores are thought to be strong ligands produced by terrestrial and marine bacteria in order to sequester Fe from their environment (Wells and Trick, 2004) whereas porphyrins, produced by almost all living organisms, are mainly present as part of the cellular debris arising from mortality and heterotrophic activity (chlorophyll, phaeophytin, hemes and other porphyrins (Hutchins et al., 1999)). The potential competing/interfering behavior of siderophores also needed to be detected as they are considered

as strong iron-complexing ligands and may outcompete porphyrins. We also needed to evaluate if other porphyrin-like molecules, uncomplexed or complexed with other metals than iron, have the potential to interfere with the chemiluminescence signal.

Three central composite designs were conducted with hemin concentrations ranging from 0, 1 and 2 nM. The final solutions were prepared in artificial seawater.

Our results indicated that none of the tested porphyrins nor the siderophores molecules interfered with the Fe-Py detection (p value < 0.001). This is in accordance with the results obtained by Vong et al. (2007). However, Suwannee River fulvic acid (SRFA) showed slight interference on the Fe-Py signal. For the Elliott Soil Fulvic Acid (ESFA) no impact was observed. To estimate the impact of ESFA and SRFA, three calibration curves were established, the first with increasing concentrations of hemin alone (0, 0.5, 0.75, 1, 1.5 nM), the second with increasing concentrations of hemin in the presence of 4500 $\mu g.l^{-1}$ of ESFA and the last with increasing concentrations of hemin in the presence of 4500 $\mu g.l^{-1}$ of SRFA. The aim was to increase the tested hemin concentrations and to observe any variation in the chemiluminescence response with the highest humic concentrations encountered in the Aulne system (4500 $\mu g.l^{-1}$, (Riso et al., 2021)). The slopes and intercepts of the three calibrations were statistically identical (P>95%, ANOVA test and slope comparison) showing that none of the humic substances interfered with Fe-Py detection (Fig. 3). We are able to predict that none of the organic substances tested here and expected in the Aulne estuary will impact the detection of Fe-Py-like complexes.

3.1.4- Colloidal Fe and particulate Fe interferences

To test the impact of colloidal Fe and particulate Fe interferences, a central composite design (CCD), using JMP software was conducted. Considering the maximum particulate iron concentration in the Aulne estuary (PFe = 4.3 $mg.l^{-1}$, S=5.2) and that 24% of this PFe corresponds to iron oxides, we tested two different concentrations of Fe_2O_3 solutions 3.25 and 6.5 $\mu mol.l^{-1}$. The CCD was completed with the addition of a $FeCl_3$ colloidal solution obtained 24 hours after dilution of $FeCl_3$ in artificial seawater. The interfering concentrations were estimated at 0.35 and 0.7 $\mu mol.l^{-1}$. This design was conducted with three different hemin concentrations: 0, 1, and 2 nM. The final solutions were all prepared in artificial seawater. Our results indicated that none of the particulate nor the colloidal solutions, tested at various concentrations, interfered with the analytical signal with and without the presence of hemin (p-value < 0.001).

3.1.5- Analytical response for powdered phytoplankton cells

The tested concentrations of the phytoplanktonic BCR sample were 225 and 450 µg.l^{-1}. The CDD performed showed that none of these concentrations impacted the blank nor the hemin signal. Moreover, none of the fresh phytoplankton samples tested were considered as Fe-Py productive, the signal obtained in the presence and absence of hemin were statistically identical for the two phytoplankton concentrations tested. (Vong, 2008) highlighted an apparent and temporary production of Fe-Py complexes during a phytoplankton monitoring experiment (*Dunaliella salina*). This production was then rapidly followed by the complete disappearance of the complexes in the medium. Here, no production was detected during the active growth phase of phytoplankton cells. The fact that no Fe-Py signal was observed in our study could arise from the difference in tested algae species and probably also in the growth phases of phytoplankton development, our experiment being performed during the growth phase of *Scrippsiella* and *pseudo nitzschia* cultures. (Vong, 2008) also showed that grazing of phytoplankton by microzooplankton can be a significant source of Fe-Py and that the latter molecules do represent cellular degradation products. Complementary studies could be conducted to detect Fe-Py production by bacterial communities as well as by grazing activities, but this remains out of the scope of this study.

3.2- Selectivity of the method

The signal response to the addition of the macromolecular bovine liver catalase and horseradish peroxidase was estimated in the presence and in the absence of the hemin standard. As explained by (Khan et al., 2014), chemiluminescence emission of the luminol-H_2O_2 system for the determination of heme proteins is highly sensitive and should also be tested for heme other than hemin. The signal for a 2-nM concentration of a single protein gave 0.53 ± 0.02 nM hemin equivalent for the catalase and 0.35 ± 0.014nM hemin equivalent for the horseradish peroxidase, both in the absence and in the presence of hemin. This can be compared to the 1.54 nM hemin equivalent signal for the catalase and 3.35 nM hemin equivalent horseradish peroxidase obtained by (Vong et al., 2007). As exposed by previous authors there is an intra-variability of the Fe-Py signal within Fe-Py which is not related to the number of Fe-Py units contained in these molecules, or to the molecular weight of these proteins. It is worth noting that the signal ratio we observed between horseradish peroxidase and bovine liver catalase is 1.5 which is relatively close to the ratio of 2.2 found by (Vong et al., 2007). However, in our case, the proteins gave lower chemiluminescence signals which cannot be explained by the addition of hydrogen peroxide. Although catalase and peroxidase are known to catalyse the dismutation reaction of this strong oxidant (Vlasits et al., 2007), the tested concentrations of both enzymes are too low compared to the concentration of the H_2O_2 stream (0.7 M). Another

439 explanation for such differences may arise from different chemiluminescence kinetics between Fe-Py
440 molecules. Nevertheless, a mixture of different Fe-Py complexes present in a sample will provide
441 different chemiluminescence responses. Unfortunately, we are not able, at this stage of
442 development, to identify the nature of the porphyrin content. That is why it is necessary to express
443 Fe-Py concentrations derived from natural samples as "nM hemin equivalent".
444

445 3.3- Figures of merits
446

447 The figures of merits of the Fe-Py method are summarised in Table 2. Figure 4 presents (a) the
448 variation of the signal intensity obtained for a 0.14 nM hemin concentration and (b) the calibration
449 curve obtained from different hemin concentrations (0, 0.07, 0.14, 0.25, 0.5, 1.25, 1.5 nM). It is
450 worth noting that intensity signals were averaged over 50 points following the addition of the
451 standard excluding the start and end artefacts.
452 For Fe-Py determination, the blank analysis was performed on buffered artificial seawater. To detect
453 the potential contribution of the buffer to the blank value, increasing volumes of the ammonium
454 buffer solution were added to a constant artificial seawater volume. The analytical response
455 corresponding to the initial volume added to the standard and sample analysis (750 µl) was
456 estimated. Thanks to the method of standard addition, buffer contribution was estimated to be 5
457 pM, which is below the detection limit (Table 2). The buffer contribution is therefore considered as
458 negligible. Additional tests were conducted using different standard matrices: artificial seawater as
459 described above, simplified artificial seawater as described in (Aminot and Kerouel, 2004) and UV-
460 irradiated natural seawater used for trace metal analysis. Calibration slopes and intercepts obtained
461 for the three media were statistically identical (p-value > 95%). The contribution of artificial seawater
462 to the blank being negligible and comparable to UV-irradiated seawater, artificial seawater was used
463 for the hemin standard preparation. The concentration of the Fe-Py complex in samples was
464 obtained by subtracting the intercept of the calibration curve from the sample voltage signal and
465 dividing the result by the calibration slope performed the same day of analysis using artificial
466 seawater.
467 The limit of detection was calculated as three times the standard deviation for the analysis of ten
468 replicates of the blank (artificial seawater with buffer addition). The detection limit was 7.2 pM, 15
469 times lower that reported by Vong et al., (2007) (110 pM). This decrease in the detection limit results
470 not only from the change in manifold architecture but also from the addition of hydrogen peroxide
471 that increases the oxidation rate of luminol.

Several works (Table 3) have quantified particulate heme b using High Performance Liquid Chromatography (HPLC) with various detection methods: Diode Array Detection (DAD) or Electrospray Ionisation (ESI) coupled with Mass spectrometry (MS) after solvent extraction. Recently (Isaji et al., 2020) developed a new sample extraction (acetone and HCl) and analysis for dissolved heme b using LC-MS/MS. HPLC-DAD-MS and LC-MS/MS present undeniable advantages in terms of sensitivity, reaching picomolar detection limits (Bellworthy et al., 2017) or lower (Louropoulou et al., 2020) enabling the analysis of most types of seawater. Our method also demonstrates good sensitivity for detecting Fe-Py-like compounds and is applicable to estuarine and coastal environments (see section 3.3). Moreover, it shows additional strengths such as low reagent and sample consumption (for one analysis: EDTA: 1.2 ml, H_2O_2 0.6 ml, luminol 0.6 ml, sample 3 ml) with no preconcentration steps that might induce analytical bias, and simplified sample handling. Finally, as it requires no rigorous extraction nor time-consuming digestion techniques, which could degrade the hemin (Hogle et al., 2014), it provides direct and fast analysis (90 s) of Fe-Py complexes in riverine, estuarine and coastal waters. Certification of the analytical method was not possible since no certified reference material of Fe-Py-like molecules exists for particulate or dissolved matrices. Inter-comparison with existing methods based on HPLC -DAD or ESI-MS could have been an alternative, if the detected compounds were identical. Unfortunately, this study aims to detect the pool of Fe-Py-like complexes and is thereby not specific, whereas the above-cited references all specifically detect the heme b molecule (Table 3).

3.4- Impact of NaN_3 addition

Instead of using $HgCl_2$ (Vong et al., 2007), the samples were poisoned with NaN_3, also known as a preservative for metal binding ligands (Cotte et al., 2018). This was done directly after sampling, by adding 3 µl of NaN_3 0.01 M to 30 ml of sample. The samples were then stored frozen at -20°C as the gap between sampling and analysis of hemin was relatively important (~6 months). To verify the impact of NaN_3 poisoning on hemin detection, the analytical response was studied on three hemin standards (1.66, 5 and 20 nM). The differences between no-addition and NaN_3 addition for the three hemin concentrations were found statistically negligible.

3.5- Method application to the Aulne estuary – Bay of Brest system

Table 4 describes the Fe-Py, Chlorophyll a (µg.l^{-1}), phaeophytin (µg.l^{-1}) and POC concentrations (mg.l^{-1}) as well as the C/N ratio (with associated pH and salinity values) obtained in the Aulne estuary- Bay

of Brest system. The unfiltered samples collected along the land-sea continuum were analysed in the laboratory after being defrosted at 4°C in dark conditions. We added 750 µl of buffer to 10 mL of sample and the solution was then analysed three times. The concentrations of Fe-Py compounds are expressed in hemin equivalent (Fig. 5). SFe and DFe samples were analysed directly in the laboratory without any sample pre-treatment.

3.5.1 Comparison with other studies

As previously reported, the exact nature of the Fe–Py complexes in seawater is unknown and consists most probably of a mixture of various heme-like ligands, biosynthesised in organisms or present in the media via cell lysis. The Fe-Py concentrations obtained for the Aulne estuary-Bay of Brest system were compared here to the results obtained by other published methods. However, the comparison should be treated with caution because of the differences in the physical speciation (dissolved or particulate) and targeted analytes of each method. Here, we measured the dissolved fraction plus the particulate reactive fraction of Fe-Py-like complexes that could encompass heme b and other iron-type porphyrins soluble enough for detection. Vong et al., (2007) also focused on Fe–Py complexes but the study involved filtered samples. Conversely, Gledhill et al., (2013) and Louropoulou et al., (2020, 2019) analysed the particulate fraction of heme b, and (Isaji et al., 2020) reported heme b in both particulate and dissolved phases.

The Fe-Py concentrations varied from 0.010±0.004 nM at S=34.9 to 1.14 ±0.03 nM at S = 5.2. They are lower than those reported by Vong et al., (2007) in the Berre pond (11.5 nM , S=22) and in the Rhône river (9.2 nM, S=0). However, they appear more consistent with the concentrations of Fe-Py observed in the Kourou river estuary (2.1 nM, S=30-34, Vong et al. 2007). At this stage, it is difficult to know whether the differences between studies are due more to analytical features or to the geographic/seasonal characteristics of the studied systems. Our values can also be compared with heme b concentrations reported for several oceanic systems. For the surface waters of the Atlantic Ocean, Louropoulou et al., (2020) reported particulate (>0.7 µm) heme b concentrations varying from 0.10 to 33.7 pM (median = 1.47 pM, n = 974). These concentrations, much lower than our values, correspond to typical open ocean waters of low turbidity and low productivity. The highest dissolved heme b concentrations reported in the literature were observed in the Gullmar Fjord (66 ± 45 pM) and were associated with a Fe concentration of 4-40 nM (Louropoulou et al., 2019). In the Tokyo Bay, (Isaji et al., 2020) reported particulate heme b concentrations as high as 0.15 nM and the heme b concentration in the dissolved phase as low as 0.006 nM. It is worth noting that the concentrations we obtained in the Bay of Brest (i.e. 0.010±0.004 nM for S=34.9 and 0.013±0.002 nM for S=34.0) stand in the same order of magnitude as those of Isaji et al. (2020). Our values in the Bay

of Brest were associated with DFe concentrations of 6 nM whereas the highest Fe-Py concentrations 1.14 ± 0.03 nM (at S = 5.2) were associated with DFe concentrations of 730 nM. DFe and SFe ranges obtained here ([DFe]: 6-730 nM, [SFe] = 4-60 nM) are similar to those commonly observed in other estuaries of the area, *i.e.* [DFe]: 12-840 nM for Penzé estuary (Riso et al., 2006) and [FeT]: 10-140 nM for the Aulne estuary (Riso et al., 2007). Fe-Py concentrations appear much lower than those of dissolved iron ([Fe-Py] = 0.1 to 1.8% of [DFe]), in line with the results of Louropoulou et al. (2020) (heme b to biogenic iron ratio of 0.2–9.1%). (Isaji et al., 2020, 2019) also found similar results in the Tokyo Bay for which the heme b concentration range in the dissolved phase (47-71 pM) corresponded to only a few percent of typical dissolved iron concentration. At our furthest point of sampling, located in the Iroise Sea and a few kilometers from the Brittany coast, the concentration obtained was under the detection limit of the method. We infer that Fe-Py concentrations decrease to subpicomolar levels towards the open ocean. Further analytical improvement will be required for Fe-Py detection at nanomolar scale for a full application to coastal and open ocean waters. The addition of a pre-concentration step would probably help to widen such application.

3.5.2 Mixing behaviour of Fe-Py compounds

Figure 5 describes the variation of Fe-Py, Chlorophyll a, phaeophytin, Particulate Organic Carbon (POC) concentrations and the Carbon over Nitrogen ratio C/N along the Aulne estuarine gradient. To our knowledge, this is the first time such a Fe-Py distribution is presented. Our results indicate that Fe-Py compounds clearly exhibit non-conservative behaviour due to several processes, other than simple mixing of riverine and marine waters. A positive anomaly (of ~40%) was first observed in the upper estuary (salinity range 2-8) corresponding to the Maximum Turbidity Zone (MTZ) where low pH values were also found (pH<7.3). These maximum concentrations of Fe-Py corresponded to the inner part of the estuary where the highest values of Chlorophyll a (1.36 $\mu g.l^{-1}$), phaeophytin (5.45 $mg.l^{-1}$) and POC (3.79 $mg.l^{-1}$) were also found in accordance with previous studies (Chauvaud et al., 2000; Queguiner and Tréguer, 1984). An important negative anomaly was detected in the salinity range 5-20, highlighting significant elimination of Fe-Py compounds following this enrichment. At salinities above 20, the Fe-Py concentrations display a conservative behaviour (Fe-Py = -0.0097S+0.348, R^2 = 0.983). A similar conservative behaviour was also displayed by DFe and SFe concentrations (not shown) indicating these Fe fractions and Fe-Py compounds are mainly diluted in the lower part of the estuary.

From salinities from 0 to 22.5, the POC/Chl*a* ratio above 200 indicates the occurrence of a degraded material from resuspension or river input (Savoye et al., 2003). For the highest salinities the POC/Chl*a* ratio was generally lower than 200 $g.g^{-1}$ displaying a high contribution of 'living' or non-

degraded phytoplankton (Table 4). The low Chl*a*/Phaeo ratios (<1) in the inner estuary (salinity between 0 and 22.5) should be related to grazing activity which could also explain the highest Fe-Py concentrations. C/N values were generally in the range 6-10, indicating that phytoplankton is the major contributor of particulate organic matter in the estuary (Liénart et al., 2017). Stronger C/N values obtained at lower salinities could argue for a more terrestrial origin influenced by other factors such as microzooplankton, heterotrophic microbes and terrestrial organisms (Huang et al., 2017). The positive anomaly of Fe-Py compounds at low salinity is probably the result of two combined processes commonly found in tidal estuaries: (1) the accumulation of particles (including those containing particulate reactive Fe-Py compounds) and/or (2) the heterotrophic activity that can potentially produce Fe-Py compounds (Servais and Garnier, 2006). Indeed, Knicker, (2004) shows that such organic matter mineralisation can lead to the production of humic-like compounds as well as amino acids, pyrimidines, purines or porphyrin structures.

Conversely, the negative deviation of Fe-Py compounds at higher salinities (22.5) associated with the strong decrease in POC and phaeophytin concentrations could correspond (1) to sedimentation of the particulate fraction containing the Fe-Py compounds in a less turbulent area of the estuary and/or (2) to flocculation of dissolved Fe-Py compounds that strongly tend to aggregate (Gledhill, 2007) as do other Fe colloids in estuaries as a result of neutralisation of their negatively charged surface by seawater cations (Sholkovitz et al., 1978).

3.5.3 Fluxes

Fluxes of Fe-Py compounds across the Aulne estuary were estimated for this specific time of the year. The linear curve drawn for the conservative part of the gradient (S>20) was used to estimate the theoretical Fe-Py concentration ($Fe\text{-}Py_{th}$). This concentration, which results from a hypothetical conservative behaviour, corresponds to the intercept of the linear curve to fluvial salinity (Delmas and Tréguer, 1983). The entering flux equals the river flow rate the day of sampling (Banque HYDRO, http://www.hydro.eaufrance.fr) multiplied by the Fe-Py concentration at S = 0 and by the molar mass of hemin considered here as the standard reference for Fe-Py complex estimation. Similarly, the net flux equals the flow rate of the river multiplied by $Fe\text{-}Py_{th}$ and by the molar mass of hemin. The loss of Fe-Py compounds within the estuary was estimated from the difference between the net flux and the entering flux. Figure 8 summarises the estimated values and the potential associated processes. The estimated entering flux through river runoff equals 240g ± 2 $g.d^{-1}$, whereas the net flux to the Iroise sea is 95 ± 10 $g.d^{-1}$ leading to a global loss of 60.2 ± 0.0%. This result indicates that the removal of Fe-Py compounds is of higher magnitude than the enrichment of Fe-Py compounds in the MTZ. The Aulne estuary globally acts as a sink for Fe-Py complexes.

4- Conclusion

Moving from a Flow Injection Analysis (FIA) technique of the initial method (Vong et al., 2007) to a Continuous Flow Analysis (CFA) with the addition of hydrogen peroxide as a reaction oxidant improved the sensitivity of the technique and expanded the linear range with rapid detection (90s/analysis). Fe-Py (dissolved + reactive particulate) distribution was reported for the first time along the land-sea continuum of the temperate macrotidal Aulne estuary (Bay of Brest, France). The Fe-Py distribution showed non-conservative behaviour due to multiple and variable modification processes in addition to the simple mixing of natural and marine waters. The related entering and removal fluxes were also estimated. The highest Fe-Py concentrations were observed in the Maximum Turbidity Zone, revealing enrichment in Fe-Py probably via resuspension of sediment. Losses of Fe-Py complexes (60%) for salinities higher than five were probably due to aggregation on the particles and to flocculation. Fe-Py concentrations decreased towards the ocean during mixing processes. Analysis of the other components of the iron cycle as part of the FeLINE project (in progress) will allow to closely link the behaviour of ligands to that of iron and to fix the balance of biogenic iron in the Aulne estuary.

The next challenge will be to study the physical speciation (particulate/colloidal/soluble fraction) of Fe-Py complexes in the Aulne estuary to better identify and distinguish the active processes between the dissolved, colloidal and particulate phases occurring in the land-sea continuum as described by (Isaji et al., 2020). Moreover, this sensitive chemiluminescence technique for the detection of Fe-Py complexes in seawater offers the potential for ship-board and coastal platform analysis as well as sensor development. Further analytical work will be required on detection limit improvement for Fe-Py detection at nanomolar scale and to widen its application to open ocean waters. In the near future, the use of this method to rapidly detect average concentrations of batch Fe-Py complexes could be a useful and complementary tool to combine with HPLC methods more focused on heme b detection in natural samples. A comparison of these two analytical methods would also be of major interest.

Author statement

Agathe Laës- Huon: Conceptualisation, Methodology, Investigation, Validation, Formal Analysis, Visualisation, Writing – original draft, Writing – review & editing, Supervision, Project administration, Funding acquisition. Romain Davy: Investigation. Léna Thomas: Investigation. Alexandre Hemery:

Methodology, Investigation, Validation, Jeremy Devesa: Investigation. Matthieu Waeles: Writing-Reviewing and Editing. Maria El Rakwe: Formal Analysis, Visualisation. Ricardo Riso: Writing – review & editing. Gabriel Dulaquais: Writing – review & editing.

Declaration of competing interest

The authors declare that they have no known competing financial interests or personal relationships that could have appeared to influence the work reported in this paper.

Alexandre Hemery training financial support was provided by DS Politique de site Ifremer funding.

Acknowledgements

This work was financially supported by “DS Politique de site” Ifremer funding (FeLINE project). Brenda Hervieu, Cedric Bouniol and Morgane Perron are acknowledged for their excellent work during analytical method development. We would like to thank Agathe Dujardin, and Marie Latimier for the phytoplankton cultures and Lylian Challier for the catalase and peroxidase interference tests. Alison Chalm is also warmly acknowledged for her linguistic editing.

5- References

Abril, G., Riou, S.A., Etcheber, H., Frankignoulle, M., De Wit, R., Middelburg, J.J., 2000. Transient, tidal time-scale, nitrogen transformations in an estuarine turbidity maximum - Fluid mud system (the Gironde, South-West France). Estuar. Coast. Shelf Sci. 50, 703–715. https://doi.org/10.1006/ecss.1999.0598

Abualhaija, M.M., Whitby, H., van den Berg, C.M.G., 2015. Competition between copper and iron for humic ligands in estuarine waters. Mar. Chem. 172, 46–56. https://doi.org/10.1016/j.marchem.2015.03.010

Aminot, A., Kerouel, R., 2004. Hydrologie des écosystèmes marins : Paramètres et analyses, Ifremer. ed.

Anderson, R.F., 2005. GEOTRACES, a global study of the marine biogeochemical cycles of trace elements and their isotopes, protocols and analytical techniques. Society 18, 18–21.

Batchelli, S., Muller, F.L.L., Chang, K.C., Lee, C.L., 2010. Evidence for strong but dynamic iron-humic colloidal associations in humic-rich coastal waters. Environ. Sci. Technol. 44, 8485–8490. https://doi.org/10.1021/es101081c

Bellworthy, J., Gledhill, M., Esposito, M., Achterberg, E.P., 2017. Abundance of the iron containing biomolecule, heme b, during the progression of a spring phytoplankton bloom in a mesocosm experiment. PLoS One 12. https://doi.org/10.1371/journal.pone.0176268

Beucher, C., Tréguer, P., Corvaisier, R., Hapette, A.M., Elskens, M., 2004. Production and dissolution of biosilica, and changing microphytoplankton dominance in the Bay of Brest (France). Mar.

Ecol. Prog. Ser. 267, 57–69. https://doi.org/10.3354/meps267057

Boiteau, R.M., Mende, D.R., Hawco, N.J., McIlvin, M.R., Fitzsimmons, J.N., Saito, M.A., Sedwick, P.N., Delong, E.F., Repeta, D.J., 2016. Siderophore-based microbial adaptations to iron scarcity across the eastern Pacific Ocean. Proc. Natl. Acad. Sci. U. S. A. 113, 14237–14242. https://doi.org/10.1073/pnas.1608594113

Bordin, G., 1991. Distribution et évolution saisonnière du cuivre dissous dans un écosystème estuarien macrotidal d'Europe occidentale (estuaire de l'Aule, France). Oceanol. Acta 14, 445–457.

Bundy, R.M., Biller, D. V., Buck, K.N., Bruland, K.W., Barbeau, K.A., 2014. Distinct pools of dissolved iron-binding ligands in the surface and benthic boundary layer of the California Current. Limnol. Oceanogr. 59, 769–787. https://doi.org/10.4319/lo.2014.59.3.0769

Bundy, R.M., Boiteau, R.M., McLean, C., Turk-Kubo, K.A., McIlvin, M.R., Saito, M.A., Van Mooy, B.A.S., Repeta, D.J., 2018. Distinct siderophores contribute to iron cycling in the mesopelagic at station ALOHA. Front. Mar. Sci. 5, 1–15. https://doi.org/10.3389/fmars.2018.00061

Chauvaud, L., Jean, F., Ragueneau, O., Thouzeau, G., 2000. Long-term variation of the Bay of Brest ecosystem: Benthic-pelagic coupling revisited. Mar. Ecol. Prog. Ser. 200, 35–48. https://doi.org/10.3354/meps200035

Cotte, L., Omanović, D., Waeles, M., Laës, A., Cathalot, C., Sarradin, P.M., Riso, R.D., 2018. On the nature of dissolved copper ligands in the early buoyant plume of hydrothermal vents. Environ. Chem. 15, 58–73. https://doi.org/10.1071/EN17150

de Baar, H.J.W., Boyd, P.W., Coale, K.H., Landry, M.R., Tsuda, A., Assmy, P., Bakker, D.C.E., Bozec, Y., Barber, R.T., Brzezinski, M.A., Buesseler, K.O., Boyé, M., Croot, P.L., Gervais, F., Gorbunov, M.Y., Harrison, P.J., Hiscock, W.T., Laan, P., Lancelot, C., Law, C.S., Levasseur, M., Marchetti, A., Millero, F.J., Nishioka, J., Nojiri, Y., van Oijen, T., Riebesell, U., Rijkenberg, M.J.A., Saito, H., Takeda, S., Timmermans, K.R., Veldhuis, M.J.W., Waite, A.M., Wong, C.S., 2005. Synthesis of iron fertilization experiments: From the iron age in the age of enlightenment. J. Geophys. Res. C Ocean. 110, 1–24. https://doi.org/10.1029/2004JC002601

Delmas, R., Tréguer, P., 1983. Evolution saisonnière des nutriments dans un ecosystème eutrophe d'Europe occidentale (La rade de Brest). Interactions marines et terrestres. Oceanol. Acta 6.

Dulaquais, G., Waeles, M., Gerringa, L.J.A., Middag, R., Rijkenberg, M.J.A., Riso, R., 2018. The Biogeochemistry of Electroactive Humic Substances and Its Connection to Iron Chemistry in the North East Atlantic and the Western Mediterranean Sea. J. Geophys. Res. Ocean. 123, 5481–5499. https://doi.org/10.1029/2018JC014211

Geider, R.J., La Roche, J., 1994. The role of iron in phytoplankton photosynthesis, and the potential for iron-limitation of primary productivity in the sea. Photosynth. Res. 39, 275–301. https://doi.org/10.1007/BF00014588

Gledhill, M., 2014. The detection of iron protoporphyrin (heme b) in phytoplankton and marine particulate material by electrospray ionisation mass spectrometry - comparison with diode array detection. Anal. Chim. Acta 841, 33–43. https://doi.org/10.1016/j.aca.2014.06.045

Gledhill, M., 2007. The determination of heme b in marine phyto- and bacterioplankton. Mar. Chem. 103, 393–403. https://doi.org/10.1016/j.marchem.2006.10.008

Gledhill, M., Achterberg, E.P., Honey, D.J., Nielsdottir, M.C., Rijkenberg, M.J.A., 2013. Distributions of particulate Heme b in the Atlantic and Southern Oceans - Implications for electron transport in phytoplankton. Global Biogeochem. Cycles 27, 1072–1082.

https://doi.org/10.1002/2013GB004639

Gledhill, M., Buck, K.N., 2012. The organic complexation of iron in the marine environment: A review. Front. Microbiol. 3, 1–17. https://doi.org/10.3389/fmicb.2012.00069

Gledhill, M., Gerringa, L.J.A., Laan, P., Timmermans, K.R., 2015. Heme b quotas are low in Southern Ocean phytoplankton. Mar. Ecol. Prog. Ser. 532, 29–40. https://doi.org/10.3354/meps11345

Gledhill, M., van den Berg, C.M.G., 1994. Determination of complexation of iron(III) with natural organic complexing ligands in seawater using cathodic stripping voltammetry. Mar. Chem. 47, 41–54. https://doi.org/10.1016/0304-4203(94)90012-4

Hassler, C.S., van den Berg, C.M.G., Boyd, P.W., 2017. Toward a regional classification to provide a more inclusive examination of the ocean biogeochemistry of iron-binding ligands. Front. Mar. Sci. 4. https://doi.org/10.3389/fmars.2017.00019

Hogle, S.L.S., Barbeau, K. a, Gledhill, M., 2014. Heme in the marine environment: from cells to the iron cycle. Metallomics 6, 1107–20. https://doi.org/10.1039/C4MT00031E

Honey, D.J., Gledhill, M., Bibby, T.S., Legiret, F.E., Pratt, N.J., Hickman, A.E., Lawson, T., Achterberg, E.P., 2013. Heme b in marine phytoplankton and particulate material from the North Atlantic Ocean. Mar. Ecol. Prog. Ser. 483, 1–17. https://doi.org/10.3354/meps10367

Huang, C., Yang, H., Lin, C., Huang, T., Zhang, M., Zhu, A., 2017. Variation pattern of particulate organic carbon and nitrogen in oceans and inland waters 1–34. https://doi.org/10.5194/bg-2017-68

Hutchins, D.A., Witter, E., Butler, A., Luther III, G.W., 1999. Competition among marine phytoplankton for different chelated iron species. Nature 400, 858–861. https://doi.org/Doi 10.1038/23680

Isaji, Y., Ogawa, N.O., Takano, Y., Ohkouchi, N., 2020. Quantification and carbon and nitrogen isotopic measurements of heme B in environmental samples. Anal. Chem. 92, 11213–11222. https://doi.org/10.1021/acs.analchem.0c01711

Isaji, Y., Takano, Y., Ogawa, N.O., Ohkouchi, N., 2019. Heme as one of the key molecules for constraining marine biogeochemical cycle. 29th Int. Meet. Org. Geochemistry, IMOG 2019 0–1. https://doi.org/10.3997/2214-4609.201903051

Johnson, K.S., Gordon, R.M., Coale, K.H., 1997. What controls dissolved iron concentrations in the world ocean? Authors' closing comments. Mar. Chem. 57, 181–186. https://doi.org/10.1016/S0304-4203(97)00047-9

Khan, P., Idrees, D., Moxley, M.A., Corbett, J.A., Ahmad, F., Von Figura, G., Sly, W.S., Waheed, A., Hassan, M.I., 2014. Luminol-based chemiluminescent signals: Clinical and non-clinical application and future uses. Appl. Biochem. Biotechnol. 173, 333–355. https://doi.org/10.1007/s12010-014-0850-1

Knicker, H., 2004. Stabilization of N-compounds in soil and organic-matter-rich sediments - What is the difference? Mar. Chem. 92, 167–195. https://doi.org/10.1016/j.marchem.2004.06.025

Laës, A., Blain, S., Laan, P., Ussher, S.J., Achterberg, E.P., Tréguer, P., de Baar, H.J.W., 2007. Sources and transport of dissolved iron and manganese along the continental margin of the Bay of Biscay. Biogeosciences 4, 181–194.

Laës, A., Vuillemin, R., Leilde, B., Sarthou, G., Bournot-Marec, C., Blain, S., 2005. Impact of environmental factors on in situ determination of iron in seawater by flow injection analysis. Mar. Chem. 97, 347–356. https://doi.org/10.1016/j.marchem.2005.06.002

767 Laglera, L.M., Tovar-Sanchez, A., Sukekava, C.F., Naik, H., Naqvi, S.W.A., Wolf-Gladrow, D.A., 2020.
768 Iron organic speciation during the LOHAFEX experiment: Iron ligands release under biomass
769 control by copepod grazing. J. Mar. Syst. 207, 103151.
770 https://doi.org/10.1016/j.jmarsys.2019.02.002

771 Laglera, L.M., Van Den Berg, C.M.G., 2009. Evidence for geochemical control of iron by humic
772 substances in seawater. Limnol. Oceanogr. 54, 610–619.
773 https://doi.org/10.4319/lo.2009.54.2.0610

774 Le pape, O., Del Amo, Y., Menesguen, A., Aminot, A., Quequiner, B., Treguer, P., 1996. Resistance of a
775 coastal ecosystem to increasing eutrophic conditions : the Bay of Brest (France), a semi-
776 enclosed zone of Western Europe. Cont. Shelf Res. 16, 1885–1907.

777 Liénart, C., Savoye, N., Bozec, Y., Breton, E., Conan, P., David, V., Feunteun, E., Grangeré, K.,
778 Kerhervé, P., Lebreton, B., Lefebvre, S., L'Helguen, S., Mousseau, L., Raimbault, P., Richard, P.,
779 Riera, P., Sauriau, P.G., Schaal, G., Aubert, F., Aubin, S., Bichon, S., Boinet, C., Bourasseau, L.,
780 Bréret, M., Caparros, J., Cariou, T., Charlier, K., Claquin, P., Cornille, V., Corre, A.M., Costes, L.,
781 Crispi, O., Crouvoisier, M., Czamanski, M., Del Amo, Y., Derriennic, H., Dindinaud, F., Durozier,
782 M., Hanquiez, V., Nowaczyk, A., Devesa, J., Ferreira, S., Fornier, M., Garcia, F., Garcia, N., Geslin,
783 S., Grossteffan, E., Gueux, A., Guillaudeau, J., Guillou, G., Joly, O., Lachaussée, N., Lafont, M.,
784 Lamoureux, J., Lecuyer, E., Lehodey, J.P., Lemeille, D., Leroux, C., Macé, E., Maria, E., Pineau, P.,
785 Petit, F., Pujo-Pay, M., Rimelin-Maury, P., Sultan, E., 2017. Dynamics of particulate organic
786 matter composition in coastal systems: A spatio-temporal study at multi-systems scale. Prog.
787 Oceanogr. 156, 221–239. https://doi.org/10.1016/j.pocean.2017.03.001

788 Liu, X., Millero, F.J., 2002. The solubility of iron in seawater. Mar. Chem. 77, 43–54.
789 https://doi.org/10.1016/S0304-4203(01)00074-3

790 Lough, A.J.M., Homoky, W.B., Connelly, D.P., Comer-Warner, S.A., Nakamura, K., Abyaneh, M.K.,
791 Kaulich, B., Mills, R.A., 2019. Soluble iron conservation and colloidal iron dynamics in a
792 hydrothermal plume. Chem. Geol. 511, 225–237.
793 https://doi.org/10.1016/j.chemgeo.2019.01.001

794 Louropoulou, E., Gledhill, M., Achterberg, E.P., Browning, T.J., Honey, D.J., Schmitz, R.A., Tagliabue,
795 A., 2020. Heme b distributions through the Atlantic Ocean: evidence for "anemic"
796 phytoplankton populations. Sci. Rep. 10, 1–14. https://doi.org/10.1038/s41598-020-61425-0

797 Louropoulou, E., Gledhill, M., Browning, T.J., Desai, D.K., Menzel Barraqueta, J.-L., Tonnard, M.,
798 Sarthou, G., Planquette, H.F., Bowie, A.R., Schmitz, R.A., LaRoche, J., Achterberg, E.P., 2019.
799 Regulation of the phytoplankton heme b iron pool during the North Atlantic spring bloom.
800 Front. Microbiol. 10. https://doi.org/10.3389/fmicb.2019.01566

801 Marie, L., Pernet-Coudrier, B., Waeles, M., Riso, R., 2017. Seasonal variation and mixing behaviour of
802 glutathione, thioacetamide and fulvic acids in a temperate macrotidal estuary (Aulne, NW
803 France). Estuar. Coast. Shelf Sci. 184, 177–190. https://doi.org/10.1016/j.ecss.2016.11.018

804 Mawji, E., Gledhill, M., Milton, J. a., Zubkov, M. V., Thompson, A., Wolff, G. a., Achterberg, E.P., 2011.
805 Production of siderophore type chelates in Atlantic Ocean waters enriched with different
806 carbon and nitrogen sources. Mar. Chem. 124, 90–99.
807 https://doi.org/10.1016/j.marchem.2010.12.005

808 Mawji, E., Gledhill, M., Milton, J. a, Tarran, G. a, Ussher, S., Thompson, a, 2008. Hydroxamate
809 siderophores: Ocurrence and importance in the Atlantic Ocean. Environ. Sci. Technol. 42, 8675–
810 8680.

811 Measures, C.I., Yuan, J., Resing, J.A., 1995. Determination of iron in seawater by flow injection

812 analysis using in-line preconcentration and spectrophotometric detection. Mar. Chem. 50, 3–
813 12. https://doi.org/10.1016/0304-4203(95)00022-J

814 Moore, C.M., Mills, M.M., Arrigo, K.R., Berman-Frank, I., Bopp, L., Boyd, P.W., Galbraith, E.D., Geider,
815 R.J., Guieu, C., Jaccard, S.L., Jickells, T.D., La Roche, J., Lenton, T.M., Mahowald, N.M., Marañón,
816 E., Marinov, I., Moore, J.K., Nakatsuka, T., Oschlies, A., Saito, M.A., Thingstad, T.F., Tsuda, A.,
817 Ulloa, O., 2013. Processes and patterns of oceanic nutrient limitation. Nat. Geosci. 6, 701–710.
818 https://doi.org/10.1038/ngeo1765

819 Muller, F.L.L., 2018. Exploring the potential role of terrestrially derived humic substances in the
820 marine biogeochemistry of iron. Front. Earth Sci. 6, 1–20.
821 https://doi.org/10.3389/feart.2018.00159

822 Obata, H., Karatani, H., Nakayama, E., 1993. Automated Determination of Iron in Seawater by
823 Chelating Resin Concentration and Chemiluminescence Detection. Anal. Chem. 65, 1524–1528.
824 https://doi.org/10.1021/ac00059a007

825 Ouddane, B., Skiker, M., Fischer, J.C., Wartel, M., 1999. Distribution of iron and manganese in the
826 Seine river estuary: Approach with experimental laboratory mixing. J. Environ. Monit. 1, 489–
827 496. https://doi.org/10.1039/a903721g

828 Queguiner, B., Tréguer, P., 1984. Studies on the Phytoplankton in the Bay of Brest (Western Europe).
829 Seasonal Variations in Composition, Biomass and Production in Relation to Hydrological and
830 Chemical Features (1981–1982). Bot. Mar. 27, 449–460.
831 https://doi.org/10.1515/botm.1984.27.10.449

832 Raimonet, M., Ragueneau, O., Andrieux-Loyer, F., Philippon, X., Kerouel, R., Le Goff, M., Mémery, L.,
833 2013. Spatio-temporal variability in benthic silica cycling in two macrotidal estuaries: Causes
834 and consequences for local to global studies. Estuar. Coast. Shelf Sci. 119, 31–43.
835 https://doi.org/10.1016/j.ecss.2012.12.008

836 Rijkenberg, M.J.A., Fischer, A.C., Kroon, J.J., Gerringa, L.J.A., Timmermans, K.R., Wolterbeek, H.T., de
837 Baar, H.J.W., 2005. The influence of UV irradiation on the photoreduction of iron in the
838 Southern Ocean. Mar. Chem. 93, 119–129. https://doi.org/10.1016/j.marchem.2004.03.021

839 Rijkenberg, M.J.A., Gerringa, L.J.A., Velzeboer, I., Timmermans, K.R., Buma, A.G.J., de Baar, H.J.W.,
840 2006. Iron-binding ligands in Dutch estuaries are not affected by UV induced photochemical
841 degradation. Mar. Chem. 100, 11–23. https://doi.org/10.1016/j.marchem.2005.10.005

842 Riso, R., Mastin, M., Aschehoug, A., Davy, R., Devesa, J., Laës-Huon, A., Waeles, M., Dulaquais, G.,
843 2021. Distribution, speciation and composition of humic substances in a macro-tidal temperate
844 estuary. Estuar. Coast. Shelf Sci. 255. https://doi.org/10.1016/j.ecss.2021.107360

845 Riso, R.D., Pernet-Coudrier, B., Waeles, M., Le Corre, P., 2007. Dissolved iron analysis in estuarine and
846 coastal waters by using a modified adsorptive stripping chronopotentiometric (SCP) method.
847 Anal. Chim. Acta 598, 235–241. https://doi.org/10.1016/j.aca.2007.07.040

848 Riso, R.D., Waeles, M., Pernet-Coudrier, B., Le Corre, P., 2006. Determination of dissolved iron(III) in
849 estuarine and coastal waters by adsorptive stripping chronopotentiometry (SCP). Anal. Bioanal.
850 Chem. 385, 76–82. https://doi.org/10.1007/s00216-006-0393-6

851 Savoye, N., Aminot, A., Tréguer, P., Fontugne, M., Naulet, N., Kérouel, R., 2003. Dynamics of
852 particulate organic matter δ15N and δ13C during spring phytoplankton blooms in a macrotidal
853 ecosystem (Bay of Seine, France). Mar. Ecol. Prog. Ser. 255, 27–41.
854 https://doi.org/10.3354/meps255027

855 Schlosser, C., Croot, P.L., 2008. Application of cross-flow filtration for determining the solubility of

iron species in open ocean seawater. Limnol. Oceanogr. Methods 6, 630–642. https://doi.org/10.4319/lom.2008.6.630

Servais, P., Garnier, J., 2006. Organic carbon and bacterial heterotrophic activity in the maximum turbidity zone of the Seine estuary (France). Aquat. Sci. 68, 78–85. https://doi.org/10.1007/s00027-005-0809-y

Sholkovitz, E.R., Boyle, E.A., Price, N.B., 1978. The removal of dissolved humic acids and iron during estuarine mixing. Earth Planet. Sci. Lett. 40, 130–136. https://doi.org/10.1016/0012-821X(78)90082-1

Tagliabue, A., Bowie, A.R., Philip, W., Buck, K.N., Johnson, K.S., Saito, M.A., 2017. The integral role of iron in ocean biogeochemistry. Nature 543, In Press. https://doi.org/10.1038/nature21058

Turner, D.R., Hunter, K.A., 2001. The Biogeochemistry of Iron in Seawater, Wiley. ed, IUPAC series on analytical and physical chemistry of environmental systems.

Ussher, S.J., Worsfold, P.J., Achterberg, E.P., Laës, A., Blain, S., Laan, P., De Baar, H.J.W., 2007. Distribution and redox speciation of dissolved iron on the European continental margin. Limnol. Oceanogr. 52. https://doi.org/10.4319/lo.2007.52.6.2530

van den Berg, C.M.G., Merks, A.G.A., Duursma, E.K., 1987. Organic complexation and its control of the dissolved concentrations of copper and zinc in the Scheldt estuary. Estuar. Coast. Shelf Sci. 24, 785–797. https://doi.org/10.1016/0272-7714(87)90152-1

Vlasits, J., Jakopitsch, C., Schwanninger, M., Holubar, P., Obinger, C., 2007. Hydrogen peroxide oxidation by catalase-peroxidase follows a non-scrambling mechanism 581, 320–324. https://doi.org/10.1016/j.febslet.2006.12.037

Völker, C., Tagliabue, A., 2015. Modeling organic iron-binding ligands in a three-dimensional biogeochemical ocean model. Mar. Chem. 173, 67–77. https://doi.org/10.1016/j.marchem.2014.11.008

Vong, L., 2008. Speciation chimique du Fer dans l'Ocean: Les complexes fer-porphyrines, méthode de détection et mécanismes de production. Université de Méditerranée Aix-Marseille II.

Vong, L., Laës, A., Blain, S., 2007. Determination of iron-porphyrin-like complexes at nanomolar levels in seawater. Anal. Chim. Acta 588, 237–244.

Vraspir, J.M., Butler, A., 2009. Chemistry of Marine Ligands and Siderophores. Ann. Rev. Mar. Sci. 1, 43–63. https://doi.org/10.1146/annurev.marine.010908.163712

Vuillemin, R., Le Roux, D., Dorval, P., Bucas, K., Sudreau, J.P., Hamon, M., Le Gall, C., Sarradin, P.M., 2009. CHEMINI: A new in situ CHEmical MINIaturized analyzer. Deep. Res. Part I Oceanogr. Res. Pap. 56, 1391–1399. https://doi.org/10.1016/j.dsr.2009.02.002

Waeles, M., Dulaquais, G., Jolivet, A., Thébault, J., Riso, R.D., 2013. Systematic non-conservative behavior of molybdenum in a macrotidal estuarine system (Aulne-Bay of Brest, France). Estuar. Coast. Shelf Sci. 131, 310–318. https://doi.org/10.1016/j.ecss.2013.06.018

Wells, M.L., Trick, C.G., 2004. Controlling iron availability to phytoplankton in iron-replete coastal waters. Mar. Chem. 86, 1–13. https://doi.org/10.1016/j.marchem.2003.10.003

Whitby, H., Bressac, M., Sarthou, G., Ellwood, M.J., Guieu, C., Boyd, P.W., 2020. Contribution of Electroactive Humic Substances to the Iron-Binding Ligands Released During Microbial Remineralization of Sinking Particles. Geophys. Res. Lett. 47. https://doi.org/10.1029/2019GL086685

Witter, A.E., Hutchins, D. a., Butler, A., Luther III, G.W., 2000. Determination of conditional stability constants and kinetic constants for strong model Fe-binding ligands in seawater. Mar. Chem. 69, 1–17. https://doi.org/10.1016/S0304-4203(99)00087-0

Worsfold, P.J., Lohan, M.C., Ussher, S.J., Bowie, A.R., 2014. Determination of dissolved iron in seawater: A historical review. Mar. Chem. 166, 25–35. https://doi.org/10.1016/j.marchem.2014.08.009

Yentsch, C.S., Menzel, D.W., 1963. A method for the determination of phytoplankton chlorophyll and phaeophytin by fluorescence. Deep. Res. Oceanogr. Abstr. 10, 221–231. https://doi.org/10.1016/0011-7471(63)90358-9

Yücel, M., Gartman, A., Chan, C.S., Luther, G.W., 2011. Hydrothermal vents as a kinetically stable source of iron-sulphide-bearing nanoparticles to the ocean. Nat. Geosci. 4, 367–371. https://doi.org/10.1038/ngeo1148

930 Figures :

931

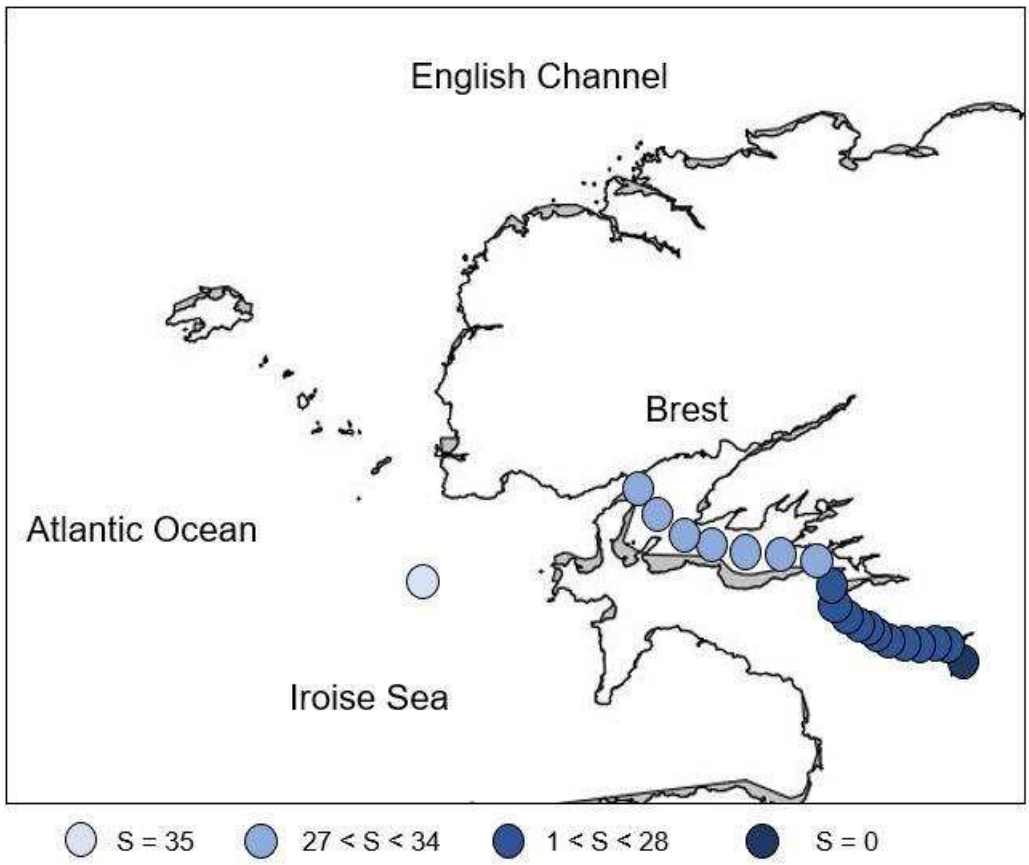

932

933 *Fig 1: Map of the study area (Western Brittany, France) with the 20 sampling points along the saline*
934 *gradient from freshwater in the Aulne, towards the Bay of Brest and finally the Iroise sea.*

935

936

937

938

939

940

941

942

943

944

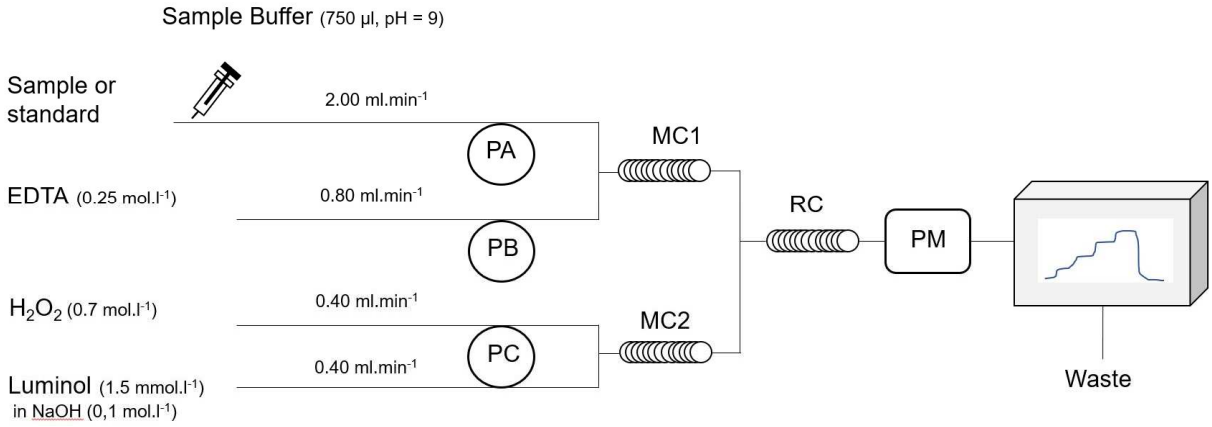

Fig. 2: Schematic view of the manifold for the Fe-Py complex determination by Continuous Flow Analysis and chemiluminescence detection (PA, PB, PC: peristaltic pumps, MC1: mixing coil 1, L=4500 mm, ID = 0.8 mm, MC2: mixing coil 2, L= 500 mm, ID = 0.8mm, RC: reaction coil, 122mm, ID = 0.8mm; PM: Photo multiplier). All the tubings were made of tygon (VWR) except the spiral cell located in front of the photomultiplier which was made of Teflon (Upchurch ID 0.8 mm).

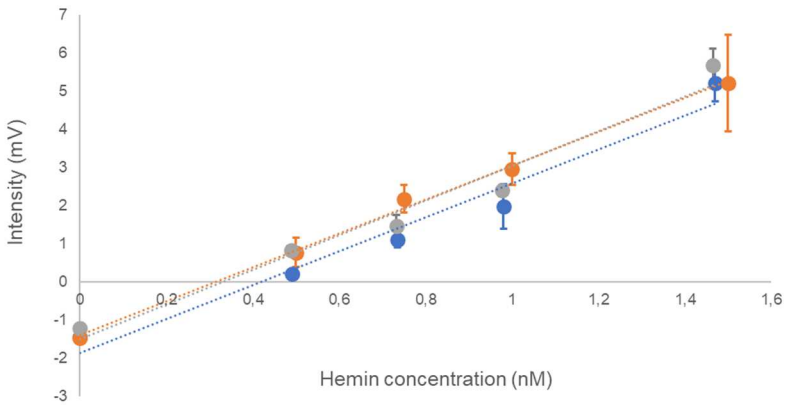

Fig. 3: Comparison of the 3 calibrations slopes for humic substances interference test (a-hemin standard calibration (0, 0.5, 0.75, 1, 1.5 nM, orange circles, y=4.44±0.14x -1.40±0.13, R^2 = 0.997, n =3), b- hemin standard calibration (0, 0.5, 0.75, 1, 1.5 nM) with addition of 4500 µg.L^{-1} of ESFA (blue circles, y=4.44±0.48x -1.86±0.43, R^2 = 0.97, n =3) and c- hemin standard calibration (0, 0.5, 0.75, 1, 1.5 nM) with addition of 4500 µg.L^{-1} of SRFA (grey circles, y=4.55±0.46x -1.51±0.40, R^2 = 0.97, n =3)

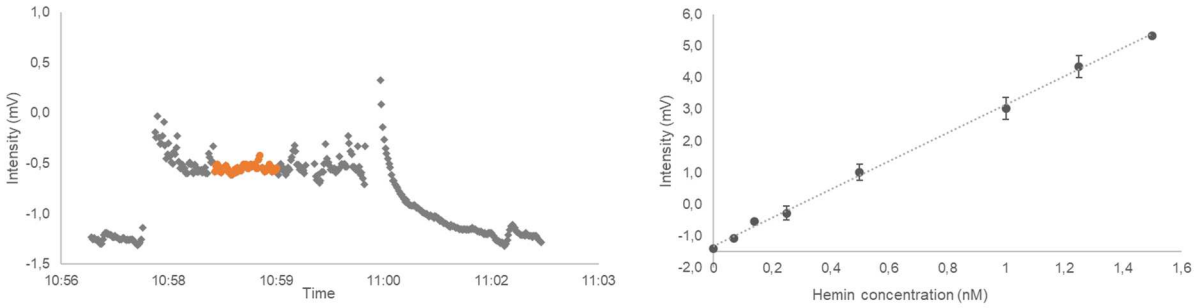

Fig. 4: a- Intensity variation (mV) over time obtained for 0.14 nM hemin complex concentration in artificial seawater using Continuous Flow Analysis (orange triangles, 50 points used for the average intensity determination), b- calibration curve for Hemin concentrations of 0, 0.07, 0.14, 0.25,0.5, 1.25, 1. 5 nM in artificial seawater (y = 4.47±0.07 -1.32±0.05, R^2 = 0.999, n=6)

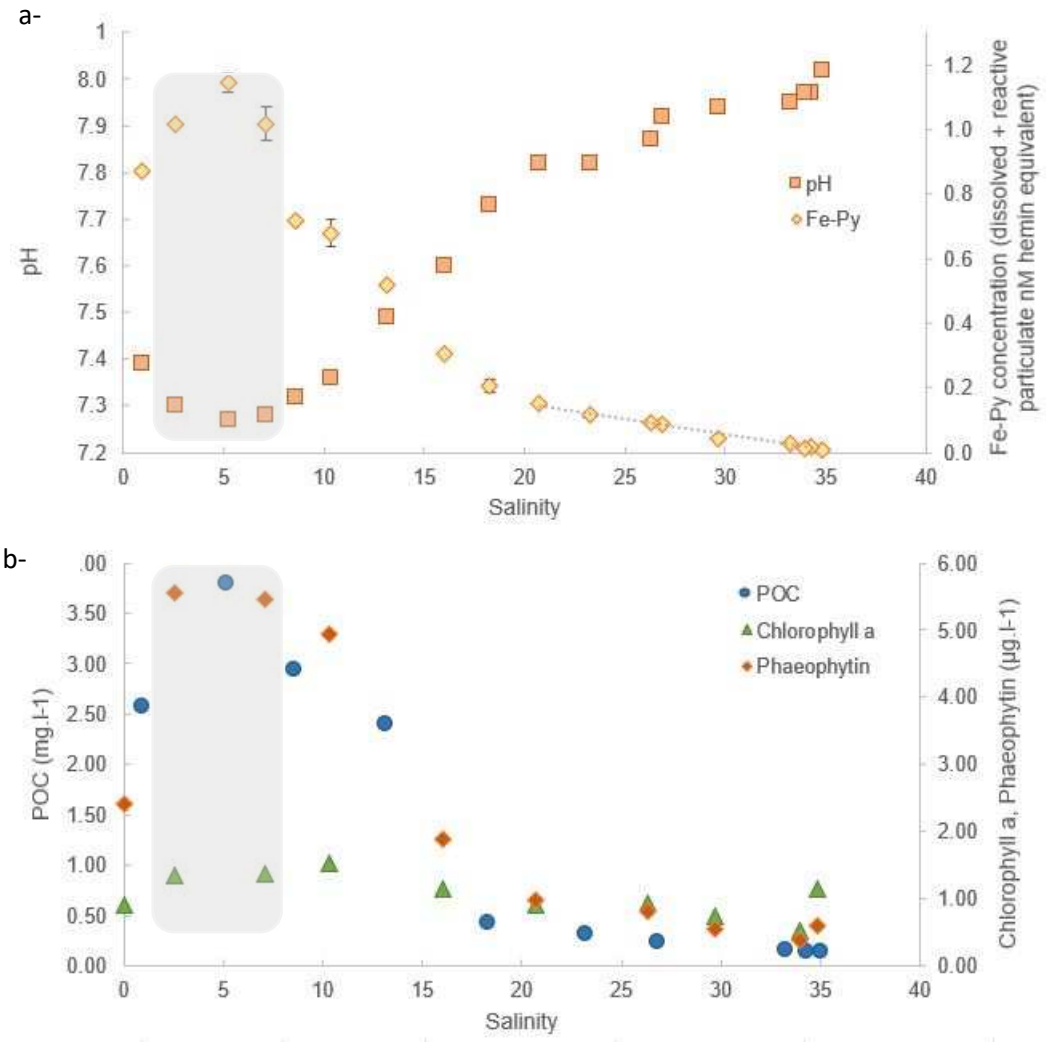

Fig. 5: a- Evolution of the concentrations of Fe–Py complexes (yellow diamonds nM hemin equivalent, n=3), pH (green squares), b- Evolution of the concentrations of POC (mg.l^{-1}, blue circles) and Chlorophyll a (µg.l^{-1}, green triangles) and phaeophytin (µg.l^{-1}, red diamonds) for the samples collected along the salinity transect of the Aulne river, estuary and Bay of Brest (shadowed rectangle: Maximum Turbidity Zone, MTZ), linear regression for the conservative part of the gradient a- Fe-Py = -0.010S+0.348, R^2 = 0.98, n= 9, Student test = 2.36

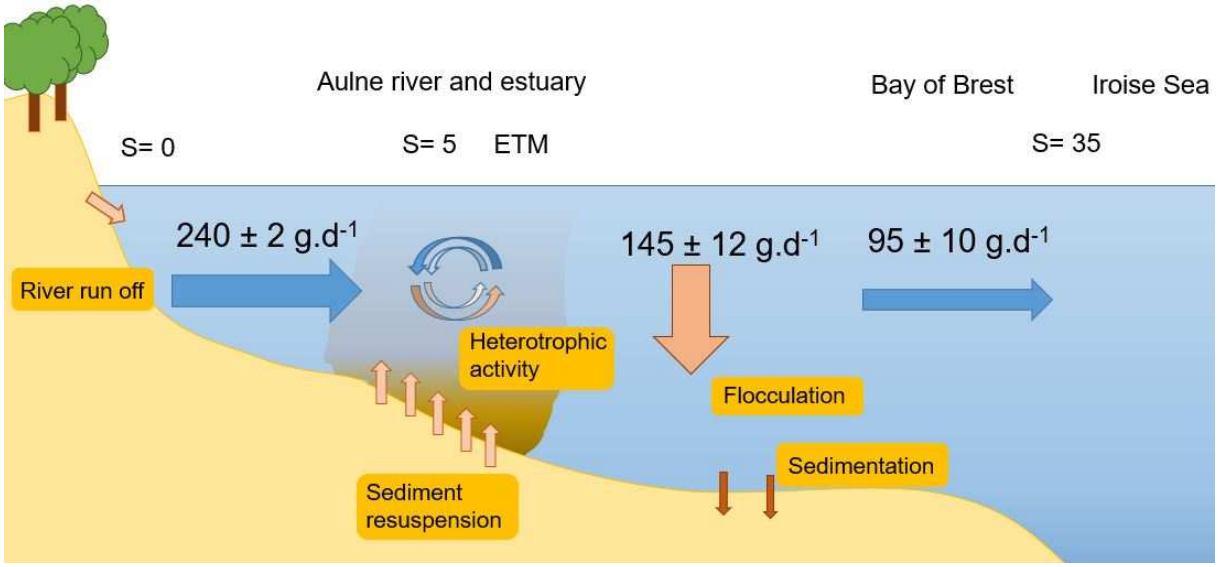

Fig. 6: Mass Balance of Fe-Py complexes and the potential associated biogeochemical processes in the Aulne Estuary-Bay of Brest system

Tables

Table 1: Various organic potential interferents, the tested concentrations in the experimental designs and the associated response

Nature of the potential interferent	Name of the compounds	Range of concentrations	Interference
Metals	Fe^{3+}	0, 350, 700 nM	None
	Fe^{2+}	0, 25, 50 nM	None
	Mn^{2+}	0, 350, 700 nM	None
	Zn^{2+}	0, 350, 700 nM	None
	Cu^{2+}	0, 50, 100 nM	None
Porphyrins	Chlorophyll a (Mg)	0, 25, 50 $\mu g.L^{-1}$	None
	Protoporphyrin IX (no metal)	0, 1, 2 nM	None
	Tetraphenylporphine Mn(III) chloride	0, 1, 2 nM	None
Siderophores	Ferrioxamine E (Fe)	0, 10, 20 pM	None
	Deferoxamine	0, 10, 20 pM	None
	Pyoverdines	0, 10, 20 pM	None
Humic Substances	Elliott Soil fulvic acid (ESFA)	0, 2250, 4500 $\mu g.l^{-1}$	None
	Suwannee River fulvic acid (SRFA)	0, 1125, 2250 $\mu g.l^{-1}$	None

Table 2: Figures of merits of the Fe-Py method

Analytical parameters	Fe-Py response
Calibration slope	$4.467*10^{+9}\pm0.069*10^{+9}$
Calibration curve intercept	-1.321±0.055
Regression coefficient	0.9986
Linearity range	0.024 – 150 nM
Detection limit (3 x sd, blank n=10)	7.2 pM
Precision (%, 0.25 nM, n=8)	6.35 %
Time of analysis	90 s

Table 3: Compilation of existing techniques for heme b or Fe-Py analysis in seawater

Reference	***Analysis time***	***Method***	***Sample pre-treatment***	***Heme detection limits when available or detection levels***	***Volume sample***	***Nature of the sample***
(Gledhill, 2007)	>1 hour	High Performance Liquid Chromatography Diode Array Spectrophotometry (HPLC-DAD)	Extraction from filtered (0.8-0.2µm) cells (2.5% octyl β-glucopyranoside in 0.02 M ammonium hydroxide), ultrasonication and centrifugation, and filtration (0.25µm) before injection	0.08 pmol or 1.57 nM (50 µL injection volume)	30-50 ml	Particulate material from phytoplankton culture
(Honey et al., 2013)	>1 hour	High Performance Liquid Chromatography Diode Array Spectrophotometry (HPLC-DAD)	For seawater samples: filtration (glass microfiber), extraction (ammoniacal EMPIGEN detergent solution), for phytoplankton cultures: extraction from filters (glass microfibers) using acid acetone (acetone:HCl) and extraction (ammoniacal detergent), for both ultrasonication, centrifugation and filtration (0.2 µm) before injection	Not indicated	2-4 l	Particulate material from batch culture and Celtic Sea and subtropical north Atlantic samples
(Gledhill et al., 2013)	>1 hour	High Performance Liquid Chromatography Diode Array Spectrophotometry (HPLC-DAD)	Filtration (0.7µm glass fiber), storage (< 80°C), extraction (0.02M NH4OH and zwitter- ionic detergent EMPIGEN), centrifugation, and filtration (0.2µm) before analysis	1.6nM	1-4 l	Particulate material from Atlantic Ocean seawater (Iceland Basin, tropical northeast Atlantic, Scotia Sea)
(Gledhill, 2014)	>1 hour	High Performance Liquid Chromatography (HPLC) Electrospray Ionisation Mass spectrometry (ESI-MS)	Filtration (0.7 µm), storage at −80°C, extraction (ammoniacal OGP), ultrasonication on ice, centrifugation and filtration (0.2 µm) before analysis	43.5±12.5 fmol (DAD) 1.2±0.5 fmol (ESI-MS)	2l	Particulate material from phytoplankton culture and seawater samples from North Atlantic
(Gledhill et al., 2015)	>1 hour	High Performance Liquid Chromatography Diode Array Spectrophotometry (HPLC-DAD), Electrospray Ionisation Mass spectrometry (ESI- MS)	Filtration (0.7µm glass fiber), extraction into ammoniacal detergent (octyl β-glucopyranoside), storage −80°C prior to analysis	Not indicated, lowest concentration detected on particulate material in culture (10±3 pM)	Not indicated	Particulate material from phytoplankton culture with Southern Ocean seawater
(Bellworthy et al., 2017)	>1 hour	High Performance Liquid Chromatography Photo-Diode Array detector (HPLC-PDA), Electrospray Ionisation Mass Spectrometer (ESI-MS)	Filtration (0.7 µm glass microfiber), storage at -80˚C, extraction into ammoniacal detergent (2.5% Octyl gluco pyranoside in 0.02 mol L-1 NH4OH), centrifugation, filtration (0.2µm) before analysis	9±8 pmol heme b L^{-1} seawater	1 l	Particulate material from Gullmar Fjord off Sweden mesocosm seawater
(Louropoulou et al., 2019)	>1 hour	High Performance Liquid Chromatography (HPLC) Electrospray Ionisation Mass spectrometry (ESI-MS)	Filtration of seawater on glass fiber filters (GF/F, pore size 0.7 µm), storage at −80 °C, extraction (w-v Octyl β-D-glucopyranoside-OGP, NH4OH), centrifugation ultrasonication on ice, and filtration (0.22µm) before analysis	0.01 to 0.02 pM for field samples	Not indicated	Particulate material from subpolar and subtropical North Atlantic Ocean seawater

(Isaji et al., 2020, 2019)	>1 hour	Ion-exchange open column chromatography, High Performance Liquid Chromatography Diode Array Spectrophotometry (HPLC-DAD) or liquid chromatography mass spectrometry (LC-MS/MS), nano-elementary analyser isotope ratio mass spectrometry (EA/IRMS)	Filtration of seawater on glass fiber filters (GF-75, pore size 0.3 µm), for biological samples and sediment frozen (-20°C) Multi-step extraction with acetone or acetone/0.5 M HCl (4:1), ultrasonication 5 min on ice and centrifugation, extraction in a 1:2 mixture of DCM and 0.1 M HCl. DCM fraction dried under Ar gas at 30 °C. For filtered seawater, 30 mL mixed with 1 mL of 12 M HCl and 6 mL of acetone, extracted three times with 6 mL of DCM. DCM fractions dried under Ar gas.	HPLC DAD: picomole level, MRM LC-MS/MS 1fM of hemin injected	30 ml for the dissolved phase	Particulate and dissolved material from coastal seawater of Tokyo Bay
(Louropoulou et al., 2020)	>1 hour	High Performance Liquid Chromatography Diode Array Detection (HPLC-DAD), Electrospray Ionisation Mass Spectrometry (ESI-MS)	Filtration of seawater on glass fiber filters (GF/F, pore size 0.7 µm), storage at −80 °C, extraction (w-v Octyl β-D-glucopyranoside-OGP), centrifugation, and filtration (0.2µm) before analysis	1.57 nM (HPLC DAD), 190 pmol heme b L^{-1} (HPLC ESI) 32 pmol heme b L^{-1} (MS)	Not indicated	Particulate material from subpolar North Atlantic to the subtropical South Atlantic seawater
(Vong et al., 2007)	3 minutes	Flow injection analysis (FIA) with chemiluminescence detection	Filtration (0.2 µm), buffer addition NH_3/NH_4 before direct injection or storage with $HgCl_2$ at -20°C, buffer addition NH3/NH4 before analysis	0.11 nM	3.5ml	Dissolved material (<0.2µm) from Guiana, Rhone and Berre river samples and phytoplankton cultures
This study	4 minutes	Continuous flow analysis (CFA) with chemiluminescence detection	Storage with NaN_2 at -20°C, buffer addition NH_3/NH_4 before analysis	7.2 pM	10ml	Dissolved and particulate material from the Aulne estuary North Atlantic seawater

Table 4: Salinity, pH, Fe-Py (nM hemin equivalent), Chlorophyll a (µg.l^{-1}), phaeophytin (µg.l^{-1}), POC concentrations (mg.l^{-1}) and C/N ratio observed along the Aulne estuary- Bay of Brest system

Sample	Salinity	pH	Fe-Py (nM hemin equivalent)	sd	Chlorophyll a (µg.l^{-1})	Phaeophytin (µg.l^{-1})	POC concentrations (mg.l^{-1})	C/N ratio
19	35.05	8.09	< LD				0.03	5.63
18	34.86	8.02	0.010	0.004	1.16	0.61		
17	34.3	7.97	0.019	0.002			0.026	6.53
16	33.98	7.97	0.013	0.002	0.53	0.39		
15	33.27	7.95	0.029	0.003			0.029	6.33
14	29.68	7.94	0.045	0.002	0.75	0.54		
13	26.83	7.92	0.087	0.003			0.043	6.74
12	26.3	7.87	0.092	0.003	0.94	0.82		
11	23.22	7.82	0.117	0.007			0.048	7.98
10	20.71	7.82	0.154	0.010	0.91	0.98		
9	18.26	7.73	0.206	0.019			0.059	8.48
8	16	7.6	0.307	0.004	1.14	1.89		
7	13.12	7.49	0.516	0.003			0.255	11.00
6	10.34	7.36	0.678	0.043	1.52	4.95		
5	8.59	7.32	0.718	0.004			0.316	10.85
4	7.1	7.28	1.016	0.054	1.36	5.45		
3	5.2	7.27	1.142	0.031			0.414	10.67
2	2.6	7.3	1.012	0.003	1.33	5.53		
1	0.92	7.39	0.873	0.007			0.292	10.30

Figure legends

Fig 1: Map of the study area (Western Brittany, France) with the 20 sampling points along the saline gradient from freshwater in the Aulne, towards the Bay of Brest and finally the Iroise sea.

Fig. 2: Schematic view of the manifold for the Fe-Py complex determination by Continuous Flow Analysis and chemiluminescence detection (PA, PB, PC: peristaltic pumps, MC1: mixing coil 1, L=4500 mm, ID = 0.8 mm, MC2: mixing coil 2, L= 500 mm, ID = 0.8mm, RC: reaction coil, 122mm, ID = 0.8mm; PM: Photo multiplier). All the tubings were made of tygon (VWR) except the spiral cell located in front of the photomultiplier which was made of Teflon (Upchurch ID 0.8 mm).

Fig. 3: Comparison of the 3 calibrations slopes for humic substances interference test (a-hemin standard calibration (0, 0.5, 0.75, 1, 1.5 nM, orange circles, y=4.44±0.14x -1.40±0.13, R^2 = 0.997, n =3), b- hemin standard calibration (0, 0.5, 0.75, 1, 1.5 nM) with addition of 4500 µg.L^{-1} of ESFA (blue circles, y=4.44±0.48x -1.86±0.43, R^2 = 0.97, n =3) and c- hemin standard calibration (0, 0.5, 0.75, 1, 1.5 nM) with addition of 4500 µg.L^{-1} of SRFA (grey circles, y=4.55±0.46x -1.51±0.40, R^2 = 0.97, n =3)

Fig. 4: a- Intensity variation (mV) over time obtained for 0.14 nM hemin complex concentration in artificial seawater using Continuous Flow Analysis (orange triangles, 50 points used for the average intensity determination), b- calibration curve for Hemin concentrations of 0, 0.07, 0.14, 0.25,0.5, 1.25, 1. 5 nM in artificial seawater (y = 4.47±0.07 -1.32±0.05, R^2 = 0.999, n=6)

Fig. 5: a- Evolution of the concentrations of Fe–Py complexes (yellow diamonds nM hemin equivalent, n=3), pH (green squares), b- Evolution of the concentrations of POC (mg.l^{-1}, blue circles) and Chlorophyll a (µg.l^{-1}, green triangles) and phaeophytin (µg.l^{-1}, red diamonds) for the samples collected along the salinity transect of the Aulne river, estuary and Bay of Brest (shadowed rectangle: Maximum Turbidity Zone, MTZ), linear regression for the conservative part of the gradient a- Fe-Py = -0.010S+0.348, R^2 = 0.98, n= 9, Student test = 2.36

Fig. 6: Mass Balance of Fe-Py complexes and the potential associated biogeochemical processes in the Aulne Estuary-Bay of Brest system

Table legends

Table 1: Various organic potential interferents, the tested concentrations in the experimental designs and the associated response

Table 2: Figures of merits of the Fe-Py method

Table 3: Compilation of existing techniques for heme b or Fe-Py analysis in seawater

Table 4: Salinity, pH, Fe-Py (nM hemin equivalent), Chlorophyll a ($\mu g.l^{-1}$), phaeophytin ($\mu g.l^{-1}$), POC concentrations ($mg.l^{-1}$) and C/N ratio observed along the Aulne estuary- Bay of Brest system

Highlights:

- Rapid and simple detection of Fe-Py complexes was developed for marine waters
- Fe-Py complexes distribution was reported for the first time in a salinity gradient
- Aulne estuary acts as a sink for Fe-Py, decreasing their input to the Atlantic Ocean